

FINAL REPORT

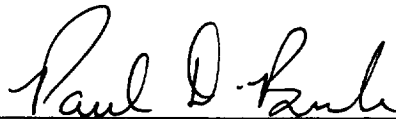
Investigation of Fiber Optics Based  
Phased Locked Diode Lasers

PHASE CORRECTION IN A SEMICONDUCTOR  
AMPLIFIER ARRAY USING FIBER OPTICS

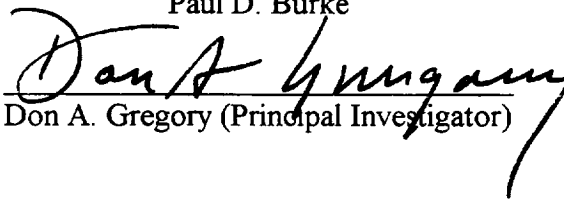
FINAL  
111 74-12  
OCT.  
11328

Period of Performance:  
March 13, 1995 to March 12, 1996

Contract No: NAS58-38609 D.O. 138



Paul D. Burke



Don A. Gregory (Principal Investigator)

Completed under:

NASA/MSFC CDDF TASK 94-23

UAH DELIVERY ORDER 138

MARCH 1997

Submitted to:

NASA/MSFC

Submitted by:

University of Alabama in Huntsville  
Department of Physics  
Huntsville, AL 35899

## **FORWARD**

This scope of work was completed under contract through the Physics Department at the University of Alabama in Huntsville, and the NASA Marshall Space Flight Center Center Director Discretionary Fund. The research completed from 3/95 to 3/96 at the Optics and RF Division was under CDDF task 94-23 at Marshall Space Flight Center in Huntsville, Alabama. The remainder of the work was completed from 3/96 to 9/96 at the Optics Building at the University of Alabama in Huntsville Physics Department. The equipment used in the experiments was property of NASA, the University of Alabama in Huntsville Physics Department, and Phillips Laboratory at Kirtland Airforce Base, Albuquerque, NM. The assistance of the NASA and University staff was vital to the completion of this project.

## TABLE OF CONTENTS

	Page
List of Figures .....	viii
List of Tables .....	x
List of Symbols .....	xi
 Chapter	
I. INTRODUCTION .....	1
1.1 Background .....	1
1.2 Power Beaming Projects .....	2
1.3 Geostationary Power Fountain .....	2
1.4 Power Beaming using an Array .....	3
1.5 Power Beaming and Coherence .....	4
1.6 Fiber Optic Phase Modulation .....	5
1.7 Coherence and Spot Size .....	5
1.8 Research Focus .....	6
II. THEORY .....	7
2.1 General Interference Theory .....	7
2.2 Phased array and diffraction theory .....	13
2.2.1 System in Cartesian Coordinates .....	13
2.2.2 Radially symmetric system in polar coordinates .....	16
2.2.3 Output power for an array with $\pi/4$ phase error .....	21

	Page
2.3 Spatial coherence theory .....	26
2.3.1 Young's Double Slit Experiment .....	27
2.3.2 Spatial coherence of an array of slits .....	29
2.3.3 Van Cittert - Zernike Theorem .....	31
2.4 Fiber Theory .....	33
2.5 Fiber interferometers and sensors .....	36
III. EXPERIMENT .....	44
3.1 Experiment Introduction .....	44
3.2 Injection Locking Semiconductor Optical Amplifiers .....	45
3.3 Fiber Based Mach Zehnder interferometer system .....	50
3.4 Piezo Electric fiber stretcher .....	51
3.5 Experimental Procedure .....	55
3.5.1 Fiber stretcher test procedure .....	57
3.5.2 Diode laser system .....	58
3.5.3 Ti : Sapphire laser test system .....	60
3.6 Experimental Results .....	63
3.6.1 Phase shift calculation .....	63
3.6.2 Mach Zehnder interferometer phase shift .....	64
3.6.3 Experiment Calculations .....	65
3.6.4 Near IR system changes .....	65
3.6.5 Amplifier output power .....	73

	Page
IV. DISCUSSION .....	79
4.1 System Considerations for Laser Power Beaming .....	79
4.2 Fiber optic phase modulation .....	80
4.3 Recommendations .....	82
4.4 Conclusion .....	83
APPENDIX A: NASA Presentation .....	85
REFERENCES .....	89
BIBLIOGRAPHY .....	92

## LIST OF FIGURES

Figure	Page
2.1    Phased Array Aperture System in Cartesian Coordinates .....	15
2.2    Phased Array Aperture System in Polar Coordinates .....	17
2.3    Mathematical model of Phased array aperture .....	23
2.4    Far-field intensity distribution of in phase array .....	24
2.5    Far-field intensity distribution of random phase array .....	25
2.6    Aperture and Observation Planes .....	28
2.7    Young's Double Slit System .....	29
2.8    Multiple Slits for Young's Experiment .....	30
2.9    Fiber Launch and TIR .....	34
2.10   Polarization Maintaining Fiber Structures .....	37
2.11   Fiber Fabry - Perot Interferometer .....	40
2.12   Fiber Sagnac Interferometer .....	40
2.13   Fiber Mach - Zehnder Interferometer .....	40
2.14   Sensing Fiber Interferometer and OPD .....	41
2.15   Phase shift and intensity in a fiber interferometer .....	42
3.1    Injection Locking Semiconductor Optical Amplifier (ILA).....	46
3.2    CIR 915 fiber stretcher and clamshell cylinder (NASA model) .....	56
3.3    CIR Fiber Stretcher Test System .....	59

Figure	Page
3.4 Ti: Sapphire laser and amplifier system for power measurements. . . . .	61
3.5 Piezo wafer expansion for test frequencies . . . . .	66
3.6 Fiber stretcher phase shift for 0-5 volts DC signal . . . . .	67
3.7 Phase shift for 5 volt amplitude with various frequencies . . . . .	68
3.8 Oscilloscope trace for stretcher - 1 kHz at 2 volt amplitude . . . . .	69
3.9 Oscilloscope trace for stretcher - 10 kHz signal at 5 volt amplitude . . . . .	69
3.10 Oscilloscope trace for stretcher - 1.6 kHz at 5 volts amplitude . . . . .	70
3.11 Oscilloscope trace for stretcher - 1 kHz at 5 volts amplitude . . . . .	70
3.12 Oscilloscope trace for stretcher - 4 kHz at 5 volts amplitude . . . . .	71
3.13 Oscilloscope trace for stretcher - 10 kHz at 2 volts amplitude . . . . .	71
3.14 Fiber Stretcher Fringe Shift Versus Frequency . . . . .	72
3.15 Fiber stretcher test interference pattern - 0 Hz . . . . .	76
3.16 Fiber stretcher test interference pattern - 20 Hz . . . . .	76
3.17 Fiber stretcher test interference pattern with extra shear . . . . .	77
3.18 Fiber stretcher test interference pattern with tilt . . . . .	77
3.19 Fiber stretcher test interference pattern - 1 kHz . . . . .	78
3.20 Fiber stretcher test interference pattern - 200 Hz . . . . .	78

## LIST OF TABLES

Table	Page
2.1 Collectable Power Loss with Phase Shift . . . . .	22
3.1 Injection Locking Amplifier Power Requirements . . . . .	48
3.2 Amplifier Power Characteristics . . . . .	49
3.3 List of System Components . . . . .	52
3.4 Fiber Stretcher Specifications . . . . .	54



## LIST OF SYMBOLS

<u>Symbol</u>	<u>Definition</u>
GPF	Geostationary Power Fountain
He-Ne	Helium Neon.
ILA	Injection locking optical amplifier.
MCF	Mutual Coherence Function.
MOPA	Master oscillator and power amplifier.
OPD	Optical path distance.
PM	Polarization maintaining.
PZT	Lead Zirconate Titanate.
Ti:Sapphire	Titanium doped Sapphire.
$a$	Radius of synthetic aperture.
$a_{\text{core}}$	Radius of fiber core.
$A$	Amplitude of electric field vector for entire array at $Z=0$ .
$A$	Source aperture at $Z=0$ .
$A_0$	Amplitude of electric field of a single emitter in aperture $A$ .
$A_{0ij}$	Amplitude of electric field of emitter (i,j) in array at $Z=0$ .
$c$	Speed of light in a vacuum. $c = 3.0 \times 10^8 \text{ m/s}^2$
$d$	Distance between two slits in Young's experiment.
$d_{ij}$	Distance between any two elements in synthetic aperture array.
$E_1(r,t), E_2(r,t)$	Electric field vector at a position $r$ and time $t$ .

<u>Symbol</u>	<u>Definition</u>
$\mathbf{E}_{ij}(q)$	Electric field vector at image plane radius $q$ from emitters in $[i,j]$ .
$E_{01}, E_{02}$	Amplitude of electric field vector $\mathbf{E}_1$ and $\mathbf{E}_2$ .
$E_{\text{total}}$	Total electric field from a sum of superimposed waves.
$e^{i\Delta\phi}$	Phase term given as $e^{i\phi_{ij} - i\phi_{ij+1}}$ .
$f_1, f_2$	Path distance from the center of $A$ to observation points in plane $P$ .
$h$	Dummy variable for calculating Bessel function, $J_1(kpq/R)$ .
$i$	Complex number, $\sqrt{-1}$ .
$i,j$	Array component identification number for array of sources.
$[i,j]$	Array from $(1,1)$ to $(i,j)$ .
$I$	Intensity of superimposed waves $\mathbf{E}_1 + \mathbf{E}_2$ .
$I_1, I_2$	Intensity of $\mathbf{E}_1$ and $\mathbf{E}_2$ respectively.
$I_0$	Intensity from a single emitter.
$I(p)$	Total intensity at point $p$ from multiple superimposed waves.
$I_0^{ij}$	Initial intensity at aperture plane from emitter $(i,j)$ in array.
$I_{\text{final}}$	Optical power out of a sensing fiber.
$I_{\text{initial}}$	Optical power into a sensing fiber.
$I_{\text{max}}$	Maximum possible intensity from a system.
$I_{\pi/4}$	Intensity at image plane with half of the sources $\pi/4$ out of phase.
$I_{\Delta\phi}$	Intensity at image plane with half of the sources $\Delta\phi$ out of phase.
$J_0(b)$	Zero order Bessel function of $(b)$ .
$J_1(b)$	First order Bessel function of $(b)$ .

<u>Symbol</u>	<u>Definition</u>
$k$	Wave number, $2\pi/\lambda$ .
$\mathbf{k}_1, \mathbf{k}_2$	Wave vectors for $\mathbf{E}_1$ and $\mathbf{E}_2$ .
$L$	Length of optical fiber.
$\Delta L$	Change in length of optical fiber.
$m$	Order number of diffraction pattern maxima.
$N$	Number of sources in array $[i,j]$ , equal to the product $ij$ .
$n_1, n_2$	Index of refraction for media 1 and 2 respectively.
$n_{\text{cladding}}$	Index of refraction of fiber cladding.
$n_{\text{core}}$	Index of refraction of fiber core.
$\Delta n$	Photo-elastic change in refractive index in a stretched fiber.
$P$	Observation plane used to calculate spatial coherence for $\Gamma_{12}(0)$ .
$P_1, P_2$	Source points in aperture plane at $Z=0$ .
$(q, \xi')$	Polar coordinates of observation plane at $Z=R$ .
$r$	Radius of synthetic aperture at $Z=0$ .
$R$	Distance along $Z$ axis between the aperture and observation planes.
$\mathbf{s}_1, \mathbf{s}_2$	Vector coordinates for source position within the aperture $A$ .
$ \mathbf{s}_1 $	$\sqrt{(x_{s1})^2 + (y_{s1})^2}$ .
$t$	Time variable.
$t'$	Time variable to include a delay in the $(\rho_2 - \rho_1)$ path difference.
$T$	Time interval over which the time average of a function is taken.
$u$	Dummy variable used to show integration of a Bessel function.

<u>Symbol</u>	<u>Definition</u>
$\gamma_{12}(0)$	Normalized degree of spatial coherence for rays from two aperture points $P_1$ and $P_2$ superimposed with no time delay ( $\tau=0$ ).
$\Gamma_{12}(0)$	Spatial coherence of waves propagating along $r_1$ and $r_2$ from $P_1$ and $P_2$ in $A$ . Same as $\Gamma(r_1, r_2, 0)$ .
$\Gamma(P_1, P_2, \tau)$	MCF for two source aperture points $P_1$ and $P_2$ with time delay $\tau$ .
$\Gamma(s, s, 0)$	Optical intensity function at aperture $A$ for a coordinate vector $s$ .
$\Gamma(\Omega_1, \Omega_2, 0)$	Spatial coherence function for two propagation paths $\Omega_1$ and $\Omega_2$ . Also used for the self coherence function with $\tau=0$ .
$\Xi$	Variable used for measuring degree of spatial coherence across a propagating beam from a synthetic aperture array of sources.
$\lambda$	Wavelength of light.
$\eta$	Dummy variable used in a zero order Bessel function integral.
$\rho_1, \rho_2$	Beam propagation paths from source points $P_1$ and $P_2$ to a point in observation plane $P$ .
$\rho_{11}$	Photo elastic tensor constant for fiber core, 0.121 for fused silica.
$\rho_{12}$	Photo elastic tensor constant for fiber core, 0.270 for fused silica.
$(\rho, \xi)$	Polar coordinates of aperture at $Z=0$ .
$\theta$	Angle of propagation from the center of an array to central peak maxima.
$\theta_1, \theta_2$	Ray angles with respect to the normal in media of index $n_1$ and $n_2$ .
$\theta_c$	Critical angle for fiber and interface of media index of $n_1$ and $n_2$ .
$\tau$	Time delay between two waves, $E_1$ and $E_2$ at an observation plane.

<u>Symbol</u>	<u>Definition</u>
$U(x,y)$	Electric field in aperture at coordinates $(x,y)$ at $Z=0$ .
$U_{ij}(x,y)$	Electric field at $(x,y)$ from emitter numbered $(i,j)$ in array at $Z=0$ .
$V^\#$	V-number, used to determine number of operable modes of a fiber.
$V(\alpha,\beta)$	Electric field of image at coordinates $(\alpha,\beta)$ at $Z=R$ .
$V_{ij}(\alpha,\beta)$	Electric field at $(\alpha,\beta)$ at $Z=R$ from a source numbered $(i,j)$ in $A$ .
$(x,y)$	Cartesian coordinates for aperture plane at $Z=0$ .
$(x_1, y_2)$	Cartesian coordinates for point in observation plane $P$ .
$(x_B, y_B)$	Cartesian coordinates for observation point at $Z=R$ .
$(x_{s1}, y_{s1})$	Coordinates of source point $P_1$ in aperture $A$ .
$z$	Separation distance from source to aperture plane.
$Z$	Longitudinal axis of propagation.
$(\alpha,\beta)$	Cartesian coordinates for image plane at $Z=R$ .
$\delta$	Piston error between $E_1$ and $E_2$ causing a phase difference.
$\Delta_\#$	Value used to calculate the $V^\#$ for a step index fiber.
$\epsilon_N$	Phase of the $N$ th wave at observation point in $z=0$ plane.
$\phi$	Phase of an electromagnetic wave or light beam.
$\phi(\Delta L)$	Phase change with a change in fiber length $\Delta L$ .
$\Delta\phi$	Phase difference.
$\Delta\phi_{ij}$	Phase difference between two emitters in the array $[i,j]$ .
$\Phi_{ij}^0$	Initial phase angle for a wave leaving an array source numbered $(i,j)$ .

<u>Symbol</u>	<u>Definition</u>
$\nu$	Frequency of light. $\nu = c/\lambda$
$\nu_p$	Poisson's ratio for a fiber core, 0.17 for fused silica.
$\omega$	Optical frequency. $\omega = 2\pi\nu$ .

## **CHAPTER I**

### **INTRODUCTION**

#### **1.1 Background**

Continuing investigations of new methods of propulsion for space vehicles are beginning to include technologies for beaming energy from the ground to space. In one concept under consideration, an intense laser beam is converted into electrical power by a photo-voltaic array, typical of those used on spacecraft today. While this is not currently used in space missions, demonstrations of the technologies needed to complete such a power beaming system are being accomplished. Earth based power beaming could be used to power orbital transfer vehicles, geosynchronous orbit satellites, or Space Station Freedom. Conversion efficiency from coherent laser light to electrical power is twice that possible in converting sunlight. Also, there is less waste heat generated in the array with laser light, making possible higher power incident beams. This could allow a ten-fold increase in converted power. Converted power could be used on board space vehicles for propulsion or payload operations. These advanced concepts have been under discussion at Marshall Space Flight Center in Huntsville, Alabama, with a recent Beamed Energy Transportation Workshop held in October 1996.

## 1.2 Power Beaming Projects

NASA's exploration of power beaming into space has led to the idea of using diode lasers for their efficiency, power, size and cost, eventually leading to conceptualization of a high power array source. Experiments began in the late 1970s (Backus, 1972) that proposed using lasers to transmit power to photovoltaic arrays. Subsequent investigations in the late 1980's considered high powered lasers for beaming to satellites and other space vehicles (Montgomery, 1995). Laser power beaming has also been pursued for use by the Department of Defense and commercial ventures as well. (Landis et al., 1992) (Landis and Westerlund, 1992) In 1990, as a result of successful power beaming studies, the SELENE project was created for space laser energy headed by John Rather and the Office of Space Access and Technology. SELENE, named after the Greek god of the moon, was proposed to use a pulsed free-electron laser and an adaptive optic segmented mirror to launch power to an orbiting satellite or lunar base. (Montgomery, 1992) (Landis et al., 1992) SELENE research was used as background for the scope of this work.

## 1.3 Geostationary Power Fountain

Phased-array power beaming is an offspring of the SELENE project. The proposed system would use a synthetic aperture phased array of emitters secured to the ground called the Geostationary Power Fountain (GPF). The adaptive optics approach is investigated in this work with a fiber optic phase correcting system. The GPF system was spawned when weaknesses in the SELENE project were more clearly defined. The GPF's primary advantages over SELENE are cost and reliability. The GPF uses many



lower power sources, and does not need a supporting structure to mount and direct it.

Phased arrays in general have the advantage of needing less support and equipment to direct a high powered beam.

Single lasers used for power beaming need a phasing or directional mirror to correct phase errors and minimize the spot size. Thermal and mechanical problems increase dramatically for steering a single source, as power beaming to space vehicles requires an optical intensity on the order of kilowatts. An array is more reliable since all elements will not fail at the same time, and it can operate continuous wave, not pulsed. like most high power lasers. Continuous wave operation is better for power conversion with photovoltaic arrays on board many satellites (Landis et al, 1992). The SELENE program proposes a pulsed free-electron laser and a directional mirror and telescope to focus it onto a lunar base from China Lake, California. Other proposed uses for SELENE's power beaming are powering space manufacturing facilities, lunar missions, and Mars missions. (Walker and Heinbockel, 1989)

#### 1.4 Power Beaming using an Array

The technology which could be the key to beaming sufficient optical power to a target in space is a synthetic aperture phased array of semiconductor sources. Phased arrays are used in radar and radio telescopes with a system of phased transmitters and receivers utilizing a synthetic aperture geometry. These systems use modulated beam phasing and source geometry to control incident spot size and location. A phased array of optical power emitters can be used for near infrared (780-860 nm) laser power beaming with the same results and control. A master oscillator and power amplifier (MOPA)

architecture would employ a laser source for the optical signal, and an array of injection-locking semiconductor optical amplifiers as the emitters. The MOPA system can use many emitters in an array to achieve a desired output power, but an adaptive optic system must be incorporated to create the phase modulation. Such an adaptive optic technology is investigated in this research using fiber optics and piezoelectric actuators.

### 1.5 Power Beaming and Coherence

A temporally coherent emitted beam is achieved by limiting the array operation to a single optical frequency with a very narrow linewidth. Multiple quantum well optical power amplifiers take an injected light beam and amplify its output. These semiconductor devices can be manufactured to operate at a specific wavelength in the near infrared. They have a narrow linewidth, and amplify only a specific incident signal wavelength. As sources in a MOPA system, they would serve as the emitting elements in a phased array. Each propagating wave from sources in an array of emitters has a different initial phase angle. Addressing the phase of each element in the array can correct phase mismatches by modulating the beam's path length in order to launch a coherent beam of light to a target vehicle in space. Modulating the phase of each beam is possible by changing its optical path distance (OPD) with respect to other beams in the array. OPD corrections can be made before final injection into the optical amplifiers. These corrections require an adaptive optic system, which is the topic of research here.

## 1.6 Fiber Optic Phase Modulation

Phase corrections to the emitted beam can be controlled using fiber optics and a fiber stretcher that changes the OPD of the light in the fiber leading to each amplifier in the aperture. Beam information from the target vehicle can be used in a fiber-optic feedback and correction system which incorporates information about beam size and degree of spatial coherence at the detector plane. Target feedback and sensor information at the array could correct phase differences before launch to optimize power collection and central peak size at the detector plane. A laser beacon could transmit atmospheric distortion information to the array site in order to make phase corrections at the array before launch.

## 1.7 Coherence and Spot Size

Propagation through the atmosphere generally changes the spatial coherence of laser beams. Geosynchronous orbit for satellites is 40 - 60 thousand kilometers, usually indicating a far field case for power beaming. Beam distortions caused by propagating through the atmosphere can be corrected by adaptive optics to shape, steer, and target the intensity pattern onto a satellite. This is accomplished by controlling the phase of the emitters in the array. Beam information from the target vehicle could allow correction of distortion at the aperture of sources. The total beam's spatial coherence will determine the size of the smallest far field diffracted spot, as well as the concentration of optical power within that spot. Power losses in the far-field pattern caused by a change of phase were modeled by Williams. (Williams, 1992) The power collection efficiency of a simulated phased array decreased very quickly with loss of phase stability beyond a

piston error of  $\lambda/5$  across the elements of the array. If a traveling beam is spatially incoherent, the central diffracted spot size can be large and the power inside diffusely distributed. Conversely, a spatially coherent beam will have a concentrated, smaller central diffraction peak with all in-phase array elements constructively interfering.

## 1.8 Research Focus

The scope of this work will begin with an overview of relevant theory for interference and optical coherence for an array of sources. An explanation of fundamental fiber optics and their applications will follow and provides added background for the components used in the experiment system, including fiber optic interferometers. The experiment will examine an adaptive optic system using a piezo electric device to stretch optical fiber. The fiber stretcher will be characterized using a fiber interferometer and various modulation frequencies. The laser beam exiting one arm of the interferometer will be amplified using a semiconductor optical amplifier. The performance of an optical amplifier will be demonstrated while the fiber stretcher changes the incident beam's phase. This will introduce the basic MOPA system with fiber optic phase modulators used as an adaptive optics system. The phased array system discussed in the GPF proposal is a candidate for application of the experimental results.

## CHAPTER II

### THEORY

#### 2.1 General Interference Theory

Interference of two beams can be seen as the superposition of waves intersecting in a common plane. For the usual case, the sources of these waves are points and are separated by a distance much greater than the wavelength of the propagating light. An interference plane at a point P a distance R away, that is much greater than the separation distance d between the sources, will sum relatively planar waves from these sources (due to a long propagation distance). Interference of two plane waves at point P is described mathematically using the principle of superposition of the electric fields of the waves. Let the scalar fields be given by:

$$E_1(r_1, t) = E_{01} \cos(\mathbf{k}_1 \cdot \mathbf{r}_1 - \omega t + \phi_1) \quad (2.1)$$

$$E_2(r_2, t) = E_{02} \cos(\mathbf{k}_2 \cdot \mathbf{r}_2 - \omega t + \phi_2) \quad (2.2)$$

$E_{01}$  and  $E_{02}$  are the amplitudes of the electric field vectors, and  $\omega$  is the frequency of oscillation.  $\mathbf{k}_1$  and  $\mathbf{k}_2$  are the wave vectors for each wave, and  $\phi_1$  and  $\phi_2$  are initial phase angles. A complex vectoral form of the fields may be written as:

$$\mathbf{E}_1 = E_{01} e^{i(\mathbf{k}_1 \cdot \mathbf{z}_1 \hat{\mathbf{z}} - \omega t + \phi_1)} \hat{\mathbf{x}} \quad (2.3)$$

$$\mathbf{E}_2 = E_{02} e^{i(\mathbf{k}_2 \cdot \mathbf{z}_2 \hat{\mathbf{z}} - \omega t + \phi_2)} \hat{\mathbf{x}} \quad (2.4)$$

Let the waves  $\mathbf{E}_1$  and  $\mathbf{E}_2$  propagate in the same direction along the Z axis with the same wavelength so that  $k_1 = 2\pi/\lambda = k_2$ , but let the path lengths be different:

$$\mathbf{k}_1 \cdot \mathbf{z}_1 \hat{\mathbf{z}} = k z_1 \quad (2.5)$$

$$\mathbf{k}_2 \cdot \mathbf{z}_2 \hat{\mathbf{z}} = k z_2 \quad (2.6)$$

$E_{01}$  and  $E_{02}$  both lie on the X axis for this example, meaning the waves are linearly polarized. Now let

$$\mathbf{E} = \mathbf{E}_1 + \mathbf{E}_2 \quad (2.7)$$

So:

$$\mathbf{E} = E_{01} e^{i(k z_1 - \omega t + \phi_1)} \hat{\mathbf{x}} + E_{02} e^{i(k z_2 - \omega t + \phi_2)} \hat{\mathbf{x}} \quad (2.8)$$

and define:

$$I = \langle \mathbf{E} \cdot \mathbf{E}^* \rangle \quad (2.9)$$

$$= \langle (\mathbf{E}_1 + \mathbf{E}_2) \cdot (\mathbf{E}_1^* + \mathbf{E}_2^*) \rangle \quad (2.10)$$

$$= \langle \mathbf{E}_1 \cdot \mathbf{E}_1^* + \mathbf{E}_2 \cdot \mathbf{E}_2^* + \mathbf{E}_1 \cdot \mathbf{E}_2^* + \mathbf{E}_2 \cdot \mathbf{E}_1^* \rangle \quad (2.11)$$

Now if only the real part of  $\mathbf{E}_1$  and  $\mathbf{E}_2$  is considered then,

$$\mathbf{E}_1 = E_{01} \hat{\mathbf{x}} \cos(k z_1 + \omega t - \phi_1) \quad (2.12)$$

$$\mathbf{E}_2 = E_{02} \hat{\mathbf{x}} \cos(k z_2 + \omega t - \phi_2) \quad (2.13)$$

$$\text{then } \mathbf{E}_1 \cdot \mathbf{E}_2^* = \mathbf{E}_2 \cdot \mathbf{E}_1^* = \mathbf{E}_1 \cdot \mathbf{E}_2 \quad (2.14)$$

and from Equation 2.11, the intensity can be written as :

$$I = \langle |\mathbf{E}_1|^2 + |\mathbf{E}_2|^2 + 2(\mathbf{E}_1 \cdot \mathbf{E}_2) \rangle \quad (2.15)$$

Taking the time average gives a value for  $I(P)$  in terms of the intensity of each of the individual sources,  $I_1$  and  $I_2$ . Let  $I_1 = \langle |\mathbf{E}_1|^2 \rangle$  and  $I_2 = \langle |\mathbf{E}_2|^2 \rangle$

$$I(P) = I_1 + I_2 + I_{12} \quad (2.16)$$

and

$$I_{12} = 2 \langle \mathbf{E}_1 \cdot \mathbf{E}_2 \rangle \quad (2.17)$$

This allows  $I_{12}$  to be called the interference term evaluated for the specific instance that  $\mathbf{E}_1$  is parallel to  $\mathbf{E}_2$ . Using this interference term, it is evident that

$$\mathbf{E}_1 \cdot \mathbf{E}_2 = E_{01} E_{02} \cos(kz_1 - \omega t + \phi_1) \cos(kz_2 - \omega t + \phi_2) \quad (2.18)$$

$$= E_{01} E_{02} \{ \cos(kz_1 + \phi_1) \cos(\omega t) + \sin(kz_1 + \phi_1) \sin(\omega t) \} \times \\ \{ \cos(kz_2 + \phi_2) \cos(\omega t) + \sin(kz_2 + \phi_2) \sin(\omega t) \} \quad (2.19)$$

Note that the time average of a function  $f(t)$  taken over a time interval  $T$  with a dummy variable  $t'$  is:

$$\langle f(t) \rangle = 1/T \int_{-\tau}^{\tau} f(t') dt' \quad (2.20)$$

$\tau$  is the period of the harmonic function  $f(t)$  and is equal to  $2\pi/\omega$ . In Equation 2.20,  $T \gg \tau$ ,

so that over a large time interval,  $1/T$  dominates the integral. The time average of

Equation 2.19 is :

$$\langle \mathbf{E}_1 \cdot \mathbf{E}_2 \rangle = 1/T \int E_{01} E_{02} [ \cos(kz_1 + \phi_1) \cos(\omega t) + \sin(kz_1 + \phi_1) \sin(\omega t) ] \times \\ [ \cos(kz_2 + \phi_2) \cos(\omega t) + \sin(kz_2 + \phi_2) \sin(\omega t) ] dt' \quad (2.21)$$

$$\begin{aligned}
&= 1/T \int E_{01} E_{02} \cos^2(\omega t) \cos(kz_1 + \phi_1) \cos(kz_2 + \phi_2) + \\
&\quad \sin^2(\omega t) \sin(kz_1 + \phi_1) \sin(kz_2 + \phi_2) + \sin(\omega t) \cos(\omega t) [\sin(kz_1 + \phi_1) \cos(kz_2 + \phi_2) + \\
&\quad \cos(kz_1 + \phi_1) \sin(kz_2 + \phi_2)] dt' \quad (2.22)
\end{aligned}$$

This expression can be simplified using the time average of two trigonometric identities,  $\langle \cos^2(\omega t) \rangle = \langle \sin^2(\omega t) \rangle = 1/2$ , and  $\langle \sin(\omega t) \cos(\omega t) \rangle = 0$ . When these are inserted into Equation 2.22, it is simplified into Equation 2.23.

$$\langle \mathbf{E}_1 \cdot \mathbf{E}_2 \rangle = E_{01} \cdot E_{02} \frac{1}{2} \cos[(kz_1 + \phi_1) - (kz_2 + \phi_2)] \quad (2.23)$$

so, using Equation 2.17,  $I_{12}$  is determined to be:

$$I_{12} = E_{01} \cdot E_{02} \cos \delta \quad (2.24)$$

(Hecht, 1991)

In Equation 2.24,  $\delta$  depends on the path length difference and initial phases.

$$\delta = [kz_1 - kz_2 + \phi_1 - \phi_2] \quad (2.25)$$

$$I_1 = \langle |\mathbf{E}_1|^2 \rangle = E_{01}^2 / 2, \quad I_2 = \langle |\mathbf{E}_2|^2 \rangle = E_{02}^2 / 2 \quad (2.26)$$

The entire expression for the interference pattern  $I$  can then be written as:

$$I = I_1 + I_2 + 2 (I_1 I_2)^{1/2} \cos \delta \quad (2.27)$$

For a system where the amplitude of each source is the same, i.e.  $E_{01} = E_{02}$ , and noting that  $I$  will have a maximum value when  $\cos \delta = 1$ , and  $I_0 = I_1 = I_2$ , bright and dark fringes (shown in terms of  $I_0$ , the intensity of a single source) occur for:

$$I(p)_{\text{maximum}} = 4 I_0 \quad \{\text{bright fringe}\} \quad \text{at } \delta = 0, \pm 2\pi, \pm 4\pi, \dots [\cos \delta = 1] \quad (2.28)$$

$$I(p)_{\text{minimum}} = 0 \quad \{\text{dark fringe}\} \quad \text{at } \delta = \pm \pi, \pm 3\pi, \dots [\cos \delta = -1] \quad (2.29)$$

(Nussbaum and Phillips, 1991)



The modulation is created by a difference in phase (caused by a difference in path lengths if the initial phase angles are equal) between the interfering waves. Light and dark fringes are created by the constructive and destructive interference of the in-phase ( $\cos\delta = 1$ ) and out of phase ( $\cos\delta = -1$ ) wavefronts.

When a large number of sources are superimposed, their wavefronts interfere as an array. The intensity in the far field can be represented as a function of the emitted intensity of a single source,  $I_0$ . Letting the electric field from each emitting source be  $E_{01} \hat{r}$  and the plane where superposition is observed be  $z=0$ , the total electric field from all of the waves in an array of  $N$  sources (originating from a single plane) with optical frequency  $\omega$  is:

$$\mathbf{E} = E_{01} [e^{i(\omega t + \epsilon_1)} + e^{i(\omega t + \epsilon_2)} + e^{i(\omega t + \epsilon_3)} + \dots + e^{i(\omega t + \epsilon_N)}] \quad (2.30)$$

$\epsilon_N$  = phase of the  $N$ th wave at an observation point in the  $z=0$  plane, due to a combination of the initial phase and the path difference.

$$\mathbf{E} = e^{i\omega t} E_{01} \hat{r} \sum e^{i\epsilon_N} \quad (2.31)$$

$$I(P) = \langle |\mathbf{E}|^2 \rangle = E_{01}^2 \langle \sum e^{-i\epsilon_N} \sum e^{i\epsilon_N} \rangle \quad (2.32)$$

$$I(P) = E_{01}^2 [1 + e^{-i(\epsilon_2 - \epsilon_1)} + e^{i(\epsilon_2 - \epsilon_1)} + 1 + e^{-i(\epsilon_3 - \epsilon_2)} + e^{i(\epsilon_3 - \epsilon_2)} + 1 + \dots] \quad (2.33)$$

$$I_0 = E_{01}^2 = \text{irradiance from one wave} \quad (2.34)$$

In the summation of the phases in Equation 2.33, there will be  $N$  terms that are equal to unity. The other terms, where  $\epsilon_1 \neq \epsilon_2$ , will be a cosine of their difference. Over the time average, there will be as many positive contributions from the cosine terms as negative ones if the phase angle  $\epsilon_N$  is random in time (due perhaps to the initial phase angle being random in time). The sum of the time averages of the electric fields is  $\langle |\mathbf{E}|^2 \rangle$ .

$$\langle |\mathbf{E}|^2 \rangle = E_{01}^2 \langle [N + 2 \cos(\epsilon_2 - \epsilon_1) + 2 \cos(\epsilon_3 - \epsilon_2) + \dots] \rangle \quad (2.35)$$

$$I_{\text{total}} = E_{01}^2 N \quad (2.36)$$

$$E = \sqrt{N} E_{01} \quad (2.37)$$

(Nussbaum and Phillips, 1991; Born and Wolf, 1975)

Equation 2.37 shows that the beam has an amplitude of  $\sqrt{N}$  times the amplitude of one wave.  $I_{\text{total}}$  is the irradiance from a sum of  $N$  emitters at a point  $P$ , all with random phases. This is essentially the result for an array of incoherent sources. If all of the sources have the same phase at the observation point, i.e.  $\epsilon_1 = \epsilon_2 = \epsilon_N = \epsilon_0$ , which can be accomplished through a suitable adjustment of initial phase angles, Equation 2.35 changes, as shown in Equation 2.38.

$$I_{\text{total}} = \langle |\mathbf{E}|^2 \rangle = E_{01}^2 \langle \sum e^{-i\epsilon_0} \sum e^{i\epsilon_0} \rangle \quad (2.38)$$

Note that  $\epsilon_0$  is the same phase for all wavefronts, and Equation 2.38 has a time averaged summation of two sums of  $N$  emitters. The total electric field amplitude,  $E$  is then:

$$\langle |\mathbf{E}|^2 \rangle = N^2 E_{01}^2 = I_{\text{total}} = N^2 I_0 \quad (2.39)$$

$$\text{Since } I_0 = \langle E_{01}^2 \rangle \quad (2.36)$$

(Nussbaum and Phillips, 1991)

Equation 2.39 shows that the summation of  $N$  in-phase, highly correlated wave fronts is a beam with the electric field amplitude of  $N^2$  sources, and thus  $N^2$  times the intensity of a single source,  $I_0$ . This can be combined with interference theory for a phased array of  $N$  emitters to demonstrate the importance of phase matched sources in an array to obtain maximum intensity output.

## 2.2 Phased array and diffraction theory

An aperture of any dimension will create a diffraction pattern according to the boundary conditions and the nature of the light that is incident upon it. A synthetic aperture creates its boundary conditions by the geometry of the sources inside the aperture. Diffraction from a synthetic aperture of radius  $a$  appears as a true illuminated aperture if the propagation distance,  $z$ , from the aperture plane is significantly large enough ( $z \gg 4a^2/\lambda$ ) (Hecht, 1991) The far-field diffraction pattern from an array of sources is then the pattern caused by an illuminated aperture of the same dimensions as the array .

### 2.2.1 System in Cartesian coordinates

For a synthetic aperture consisting of an array of  $N$  sources numbered from  $(1,1)$  to  $(i,j)$ , with  $N = (i \cdot j)$ , the far field irradiance pattern is given by the Fraunhofer diffraction pattern of the array's aperture, with a phase contribution from the piston error of each emitter. The resulting beam's phase error is the combination of the piston errors from the emitted beams in the entire array.

A system to demonstrate the diffraction pattern for this array is defined with  $(x, y)$  as the aperture plane coordinates, and  $(\alpha, \beta)$  as image plane coordinates with a common  $Z$  axis along the normal to both planes, which also acts as the axis of propagation connecting the origins of both planes. This system is shown in Figure 2.1.

The electric field of the entire array at  $z=0$  is  $U(x,y)$ , traveling to the image plane over a distance  $R$  separating the aperture and image planes. The electric field from the aperture at the far field image plane is  $V(\alpha, \beta)$ . Finding  $V_{ij}(\alpha, \beta)$  at the image plane is done by propagating the sum of the electric fields  $U_{ij}(x,y)$  in the array to the image plane at  $R$ .

$$V_{ij}(\alpha, \beta) = \frac{e^{i(kR - \alpha x + \phi)}}{R} \iint_A U(x, y) e^{\frac{ik(\alpha x + \beta y)}{R}} dx dy \quad (2.40)$$

$$k = 2\pi/\lambda$$

$$\omega = \text{optical frequency}$$

$$\phi = \text{phase angle} \quad (\text{Hecht, 1992})$$

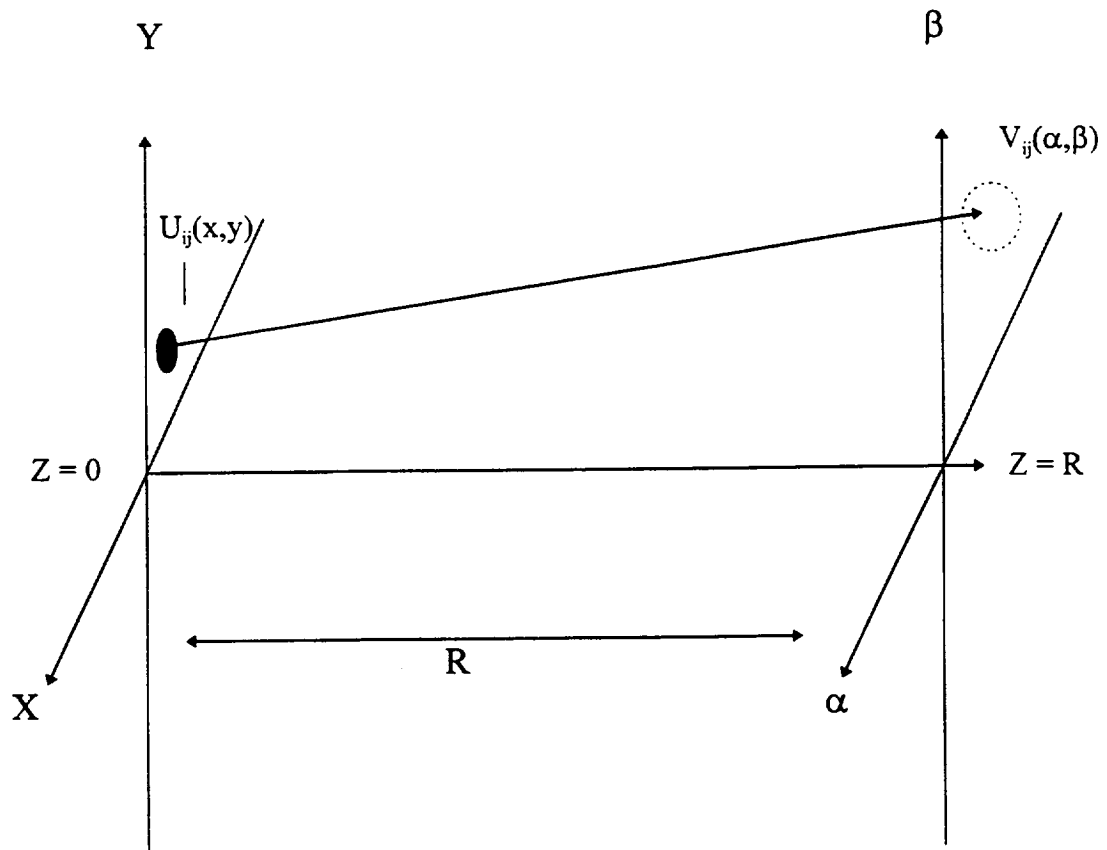


Figure 2.1 Phased Array Aperture System in Cartesian Coordinates

### 2.2.2 Radially symmetric system in polar coordinates

Changing Equation 2.40 to polar coordinates uses the radial symmetry of the system. This is accomplished changing  $U(x,y)$  to  $U(\rho,\xi)$ , and  $V_{ij}(\alpha,\beta)$  to  $V_{ij}(q,\xi')$ . The radius of the aperture at  $Z=0$  is  $a$ . The distance between the aperture and observation planes is still  $R$ . Using a trigonometry identity for the radial symmetry of the system, shown as Equation 2.42, and inserting  $U(x,y) = A$  for a uniform electric field amplitude across the emitters within the aperture radius vector  $a$ , Equation 2.43 is much more usable. Figure 2.2 shows the system with polar coordinates.

$$x = \rho \cos \xi \quad y = \rho \sin \xi \quad z = z \quad \alpha = q \cos \xi' \quad \beta = q \sin \xi'$$

$$V_{ij}(q, \xi') = e^{i(kR - \omega t + \phi)} (1/R) \int_{\rho=0}^{\rho=a} \int_{\phi=0}^{\phi=2\pi} A e^{ik\rho q/R (\cos \xi \cos \xi' + \sin \xi \sin \xi')} \rho d\rho d\xi \quad (2.41)$$

$$\cos \xi \cos \xi' + \sin \xi \sin \xi' = \cos (\xi - \xi') \quad (2.42)$$

$$V_{ij}(q, \xi') = \frac{e^{i(kR - \omega t + \phi_{ij})} A}{R} \int_{\rho=0}^{\rho=a} \rho d\rho \int_{\xi=0}^{\xi=2\pi} e^{i(\frac{k\rho q}{R})(\cos(\xi - \xi'))} d\xi \quad (2.43)$$

(Hecht, 1992)

The rotational symmetry of the system allows the  $\xi'$  term to be zero, since any value of  $\xi'$  will give the same result. This integral allows the zero-order Bessel function identity for  $J_0(\eta)$  to be inserted into Equation 2.43 as shown in Equation 2.44 using  $\eta$  as a dummy variable.

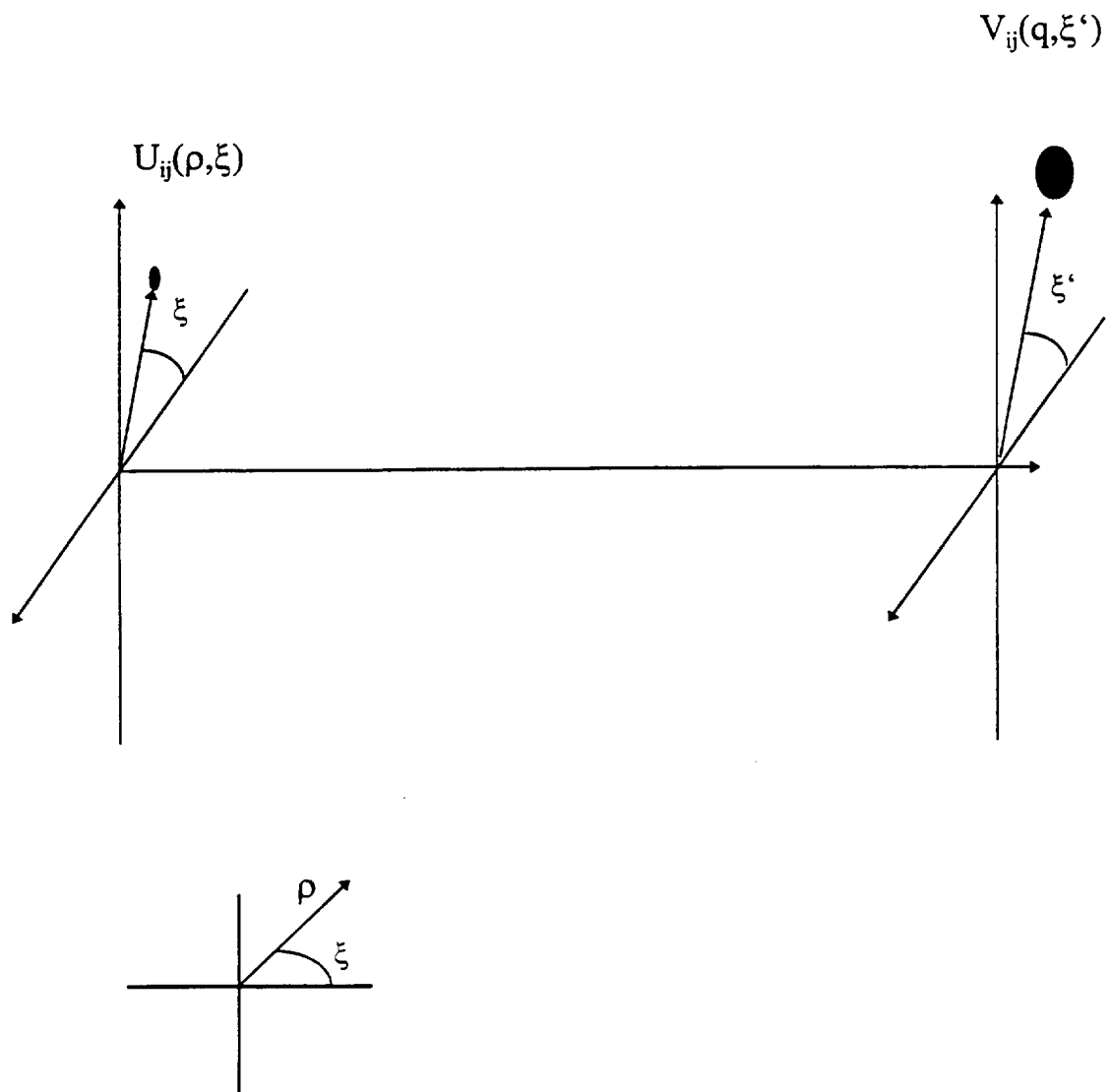


Figure 2.2 Phased Array Aperture System in Polar Coordinates

Substituting Equation 2.44 into equation 2.43 for the Bessel function integral result gives

$V_{ij}(\alpha, \beta)$  as a function of aperture and propagation dimensions in Equation 2.45.

$$J_0(\eta) = (1/2\pi) \int_0^{2\pi} e^{i\eta \cos\phi} d\phi \quad (2.44)$$

$$V_{ij}(\alpha, \beta) = \frac{A}{R} e^{i(kR - \omega t + \phi_{ij})} \int_0^a \rho [2\pi J_0(k\rho q/R)] d\rho \quad (2.45)$$

(Born and Wolf, 1975)

This expression can be changed to a first order Bessel function using the same integral method in Equation 2.44 letting  $h = k\rho q/R$ .

$$\rho = h (R/kq)$$

$$d\rho = dh (R/kq) \quad (2.46)$$

$$\int_0^h u' J_0(u') du = h[J_1(h)] \quad (2.47)$$

$$\int_0^a \rho [2\pi J_0(k\rho q/R)] d\rho = 2\pi(R/kq)^2 \int_{h=0}^{h=k\rho q/R} J_0(h) h dh \quad (2.48)$$

$$= 2\pi \int J_0(k\rho q/R) \rho d\rho$$

$$= 2\pi (R/kq)^2 J_1(kaq/R) \quad (2.49)$$

$$V_{ij}(\alpha, \beta) = \frac{A}{R} e^{i(kR - \omega t - \phi_{ij})} \left(\frac{R}{kq}\right)^2 2\pi \left(\frac{kaq}{R}\right) J_1\left(\frac{kaq}{R}\right) \quad (2.50)$$

$$= 2 \frac{A}{R} e^{i(kR - \omega t + \phi_{ij})} (\pi a^2) \left(\frac{R}{kaq}\right) J_1\left(\frac{kaq}{R}\right) \quad (2.51)$$

$$= 2 \frac{A}{R} e^{i(kR - \omega t)} e^{i\Delta\phi} Area_{emitter} \frac{J_1\left(\frac{kaq}{R}\right)}{\left(\frac{kaq}{R}\right)} \quad (2.52)$$

(Hecht, 1992)



The expression  $e^{i\Delta\phi}$  is the phase dependent term of the beams from the array. This will become a determinate of the in-phase incident power as  $\cos(\Delta\phi)$  when the intensity is taken from the electric field equation, as  $I = 1/2(\mathbf{E} \cdot \mathbf{E})$ . Superposition of waves with a phase error will cause them to interfere somewhat destructively, lowering the overall intensity in the diffraction pattern incident on the image plane. A phase-matched array will have no phase errors, and all sources in the aperture will contribute to the intensity as shown in Equation 2.39 with the total output power proportional to  $N^2$  times the power from one emitter in the aperture. The net phase factor of the array can be expressed as sum of piston errors in Equation 2.53.

$$\Sigma_{ij} e^{i\Delta\phi_{ij}} = 1/2 [ 1 + \cos ( kd_{ij}\sin\theta + \Phi_{ij}^0 ) ] \quad (2.53)$$

In Equation 2.53,  $d_{ij}$  is the separation of array element  $[i,j]$  and the reference path used to compare the phase. The  $\Phi_{ij}^0$  term is the initial phase angle; however, this can be incorporated into the piston error for the  $[i,j]$  emitter by changing its value of  $d_{ij}$  accordingly.

A difference in phase from beams at  $(i, j)$  and  $(i, j+1)$  is a piston error between the two. For  $N$  emitters in  $[i \times j]$ , the electric field at the image plane changes to  $E_{ij}(q, \xi')$  with a switch to polar coordinates. Letting the electric field amplitude from each source in the aperture be  $A^0$ , then

$$E_{ij}(q) = \Sigma_{ij} \{ E(\text{aperture's diffraction pattern}) \cdot (\text{beam phase}) \}$$

$$\Sigma E_{ij}(q) = \frac{A_{ij}^0}{R} \text{Area}_{array} e^{i(kR - \omega t)} \frac{J_1\left(\frac{kaq}{R}\right)}{\left(\frac{kaq}{R}\right)} \{1 + \cos(kd_{ij} \sin \theta)\} \quad (2.54)$$

Note that  $q/R = \sin\theta \approx \theta$ , especially for long propagation distances  $R$ . This assumption changes Equation 2.54 making all of the beam angles from the array very small.

$$\Sigma E_{ij}(\theta) = Area \frac{A_{ij}^0}{R} e^{i(kR - \omega t)} \frac{J_1(ka\theta)}{(ka\theta)} \{1 + \cos(kd_{ij}\theta)\} \quad (2.55)$$

$$\begin{aligned} I(\theta) &= 1/2 \{E^*E\} \\ &= (1/2)(Area)^2 \Sigma_{ij} A_{ij}^0 \left( \frac{J_1(ka\theta)}{(ka\theta)} \right)^2 \{1 + \cos(kd_{ij}\theta)\}^2 \end{aligned} \quad (2.56)$$

For an on-axis, synthetic aperture phase-locked array, Equation 2.56 is a pattern with a large peak central diffraction lobe. An array of phased sources along a line path creates an Airy disk pattern, however an actual aperture has a much more complex intensity distribution with side lobes and a central peak. The  $1/2[1 + \cos(kd\theta)]^2$  phase term in Equation 2.56 modulates the constructive interference in the central lobe of the pattern, including the lobe diameter and percentage of incident power in the lobe. The value of this term will change between 1 and 0 with changes in  $d$  and  $\theta$ . If every other source in an array is out of phase by  $\pi$  radians when comparing adjacent array sources, complete destructive interference would cause the central lobe to have close to zero power difference as compared to surrounding points in the image plane. This image plane would look dimly illuminated with uniformly incoherent light, typical of an out of phase array.

Phase differences cause power losses even if only a few of the sources are out of phase. This can be shown with a simple model array demonstrating the power collection at an image plane as a function of the phase errors in the beams from an array aperture of

sources. An array whose sources are either in phase, or  $\pi/4$  out of phase can be modeled for total incident power to further demonstrate the importance of phase locked operation. In doing so, the diffraction pattern at the image plane is left out of the calculation since the power distribution is not needed for finding the destructive interference caused by phase errors. The model is for an array numbered from [1,1] to [i,j].

### 2.2.3 Output power for an array with $\pi/4$ phase error

$$E = \sum_i \sum_j A_{0ij} [1 + \cos kd_{ij} \sin \theta_{ij}] \quad (2.57)$$

$$I = \frac{1}{2} [\text{Area}_{\text{aperture}}]^2 \sum_{i,j} [A_0^{ij}] [1 + \cos(\Delta\phi_{ij})] \quad (2.58)$$

$$I = \frac{\text{Area}^2}{2} \left\{ \sum_{i,j}^{\Delta\phi=0} A_0^{ij} (1 + \cos \Delta\phi) + \sum_{i,j}^{\Delta\phi=\frac{\pi}{4}} A_0^{ij} (1 + \cos \Delta\phi) \right\} \quad (2.59)$$

$$\frac{I_{\Delta\phi=\frac{\pi}{4}}}{I_{\text{in-phase}}} = \frac{I_0^{ij} \left[ \frac{ij}{2} (4) + \frac{ij}{2} (1 + \frac{\sqrt{2}}{2})^2 \right]}{I_0^{ij} [ij(4)]} \quad (2.60)$$

$$\frac{I_{\Delta\phi=\frac{\pi}{4}}}{I_{\text{in-phase}}} = \frac{\frac{ij}{2} (6.914213)}{ij(4)} \quad (2.61)$$

Equation 2.61 is a ratio for the out of phase to in-phase collected power. Table 2.1 shows how the ratio can change for various phase differences, demonstrating how the total output is affected by destructive interference.

Phase Error ( $\Delta\phi$ )	$\frac{I_{\Delta\phi}}{I_{\max}}$
$\pi/2$	0.625
$\pi/4$	0.864
$\pi/5$	0.909
$\pi/10$	0.976

Table 2.1 Collectable Power Loss with Phase Shift

Williams' (Williams, 1992) computer simulation of a phased array shows the far-field central lobe diffraction pattern for a synthetic aperture array propagating a distance comparable to a satellite orbit distance ( $10^4$  km). The central lobe intensity patterns are modeled for an in phase and a random phase array. The random phased array has a central peak intensity and lobe diameter which are much worse for efficient power transmission than for the in phase model. The intensity distributions from this model clearly shows that an in phase array has a narrow central peak. Results are shown as Figures 2.3, 2.4, and 2.5. The change of peak power and lobe size with the array's phase change verifies the necessity of adaptive optics in a power beaming architecture.

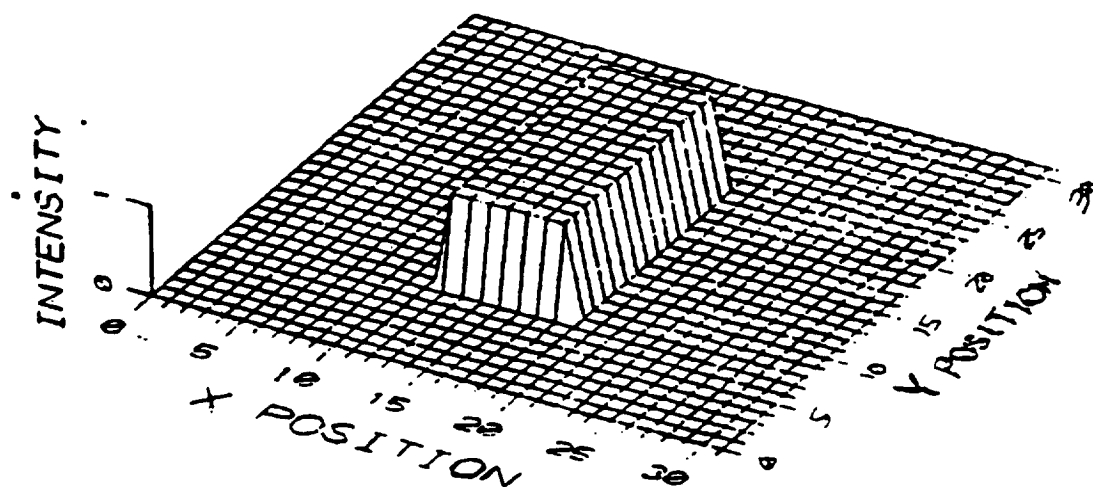


Figure 2.3 Mathematical model of Phased array aperture

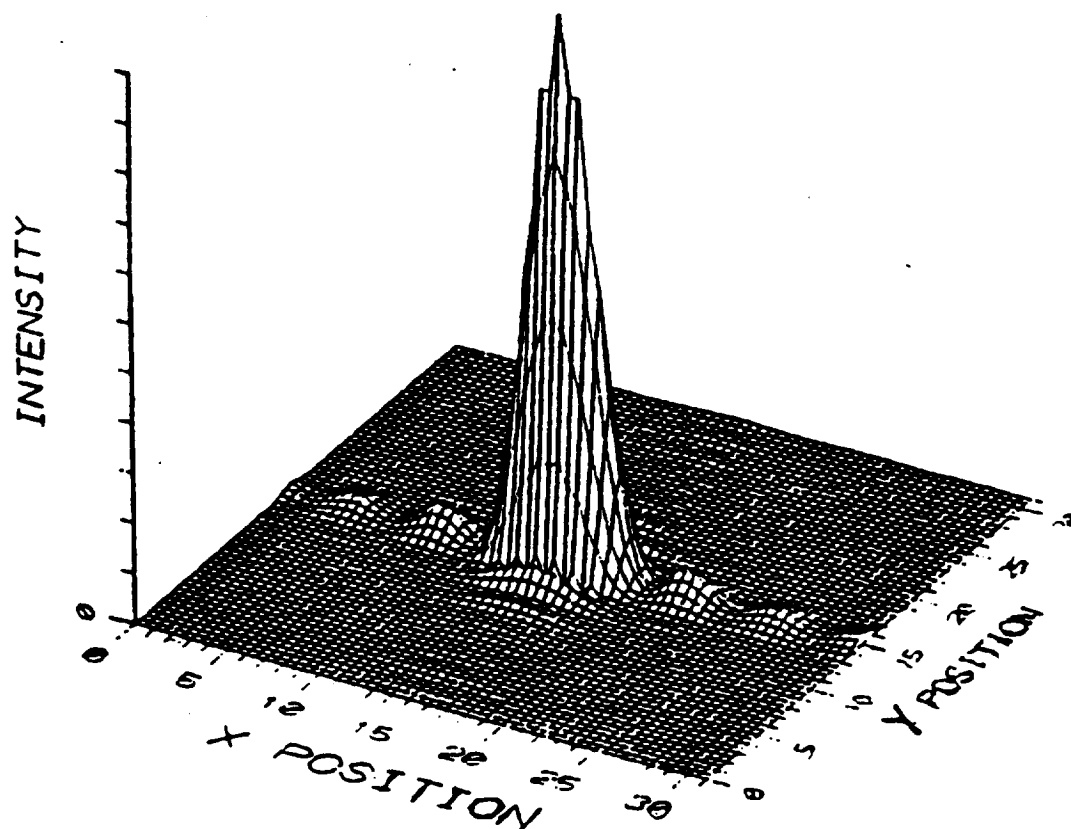


Figure 2.4 Far-field intensity distribution of in phase array

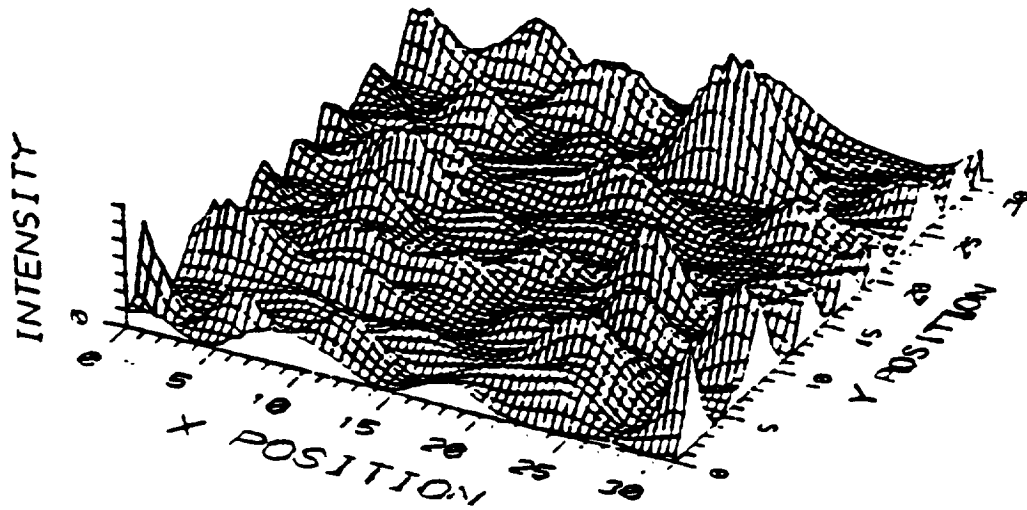


Figure 2.5 Far-field intensity distribution of random phase array

### 2.3 Spatial Coherence Theory

A beam of light traveling from an aperture to an observation plane has a wave front phase profile that, in general, changes while propagating. Piston errors across the beam and variances in the frequency of the source determine the degree of coherence. The spatial coherence of propagating light is determined by measuring how beams leaving two points in an aperture correlate at an observation plane along the direction of travel. The degree of spatial coherence is a subset of the mutual coherence function (MCF), shown as Equation 2.62, which describes the temporal and spatial coherence of propagating light. The MCF uses spatial coherence information with a time delay between two beams to compare their monochromaticity over time. Spatial coherence uses a time delay of zero, so that the correlation of the spatial relationship between two rays can be described as a phase delay at the same observation plane.

$$\Gamma(P_1, P_2, \tau) = \langle V(P_1, t' + \tau) V^*(P_2, t') \rangle \quad (2.62)$$

$$= \lim_{T \rightarrow \infty} \frac{1}{2T} \int_{-T}^T V(P_1, t' + \tau) V^*(P_2, \tau) dt' \quad (2.63)$$

(Marathay, 1982)

$P_1$  and  $P_2$  are points in the aperture plane, and  $V(P_1, t)$  is the electric field equation for a wave leaving from  $P_1$ . The distance  $V(P_1, t)$  travels during a time  $t$  is given as  $\rho_1$ . A time delay  $\tau$  is defined in Equation 2.64 for a difference in ray path lengths  $\rho_1$  and  $\rho_2$ . Also, the extra time it takes light from  $P_2$  to catch up to  $P_1$  and reach the observation plane is given as  $t'$  in Equation 2.65.



$$\tau = \frac{\rho_2 - \rho_1}{c} \quad (2.64)$$

$$t' = t - \frac{\rho_2}{c} \quad (2.65)$$

The spatial coherence function, also called the mutual optical intensity (MOI) function describes the phase across a beam of light. A correlation function is created for two rays,  $\rho_1$  and  $\rho_2$ , which travel to the same observation plane from different initial points in a source aperture,  $A$ . The MOI function can be used with the Young's double slit experiment to describe the spatial coherence of two beams leaving from the same source aperture. If waves from the aperture are not in phase, they are spatially incoherent. (Marathay, 1982)

### 2.3.1 Young's Double Slit Experiment

In the coordinate planes for describing the spatial coherence of an illuminated double slit system,  $\mathbf{f}_1$  and  $\mathbf{f}_2$  have components  $(x_1, y_1)$  and  $(x_2, y_2)$  in an observation plane at  $Z = z_1$ .  $s_1, s_2$  are aperture variable coordinates for points  $P_1$  and  $P_2$  in the source aperture  $A$ . In this case, the two points lie in two slits separated by a distance  $d$ . The aperture is located at  $Z=0$ . This system is shown in Figure 2.6. The planes are assumed to be perpendicular and the direction of propagation from one plane to the other is along a perpendicular to the aperture plane. Also, the light is assumed to be linearly polarized and propagates as a plane wave. These assumptions can be used for a quasi-monochromatic source, (for use in a temporally coherent field  $\Delta\nu \ll \nu$ ) which closely resembles real laser sources.

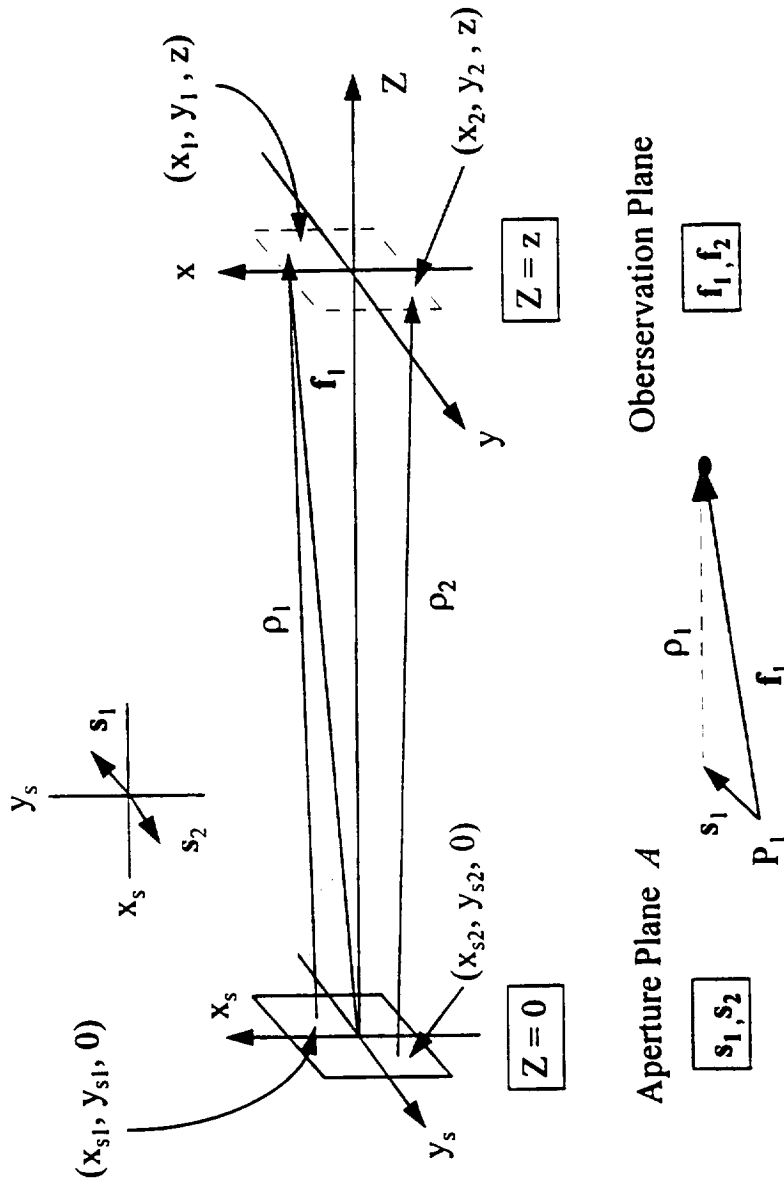


Figure 2.6 Aperture and Observation Planes

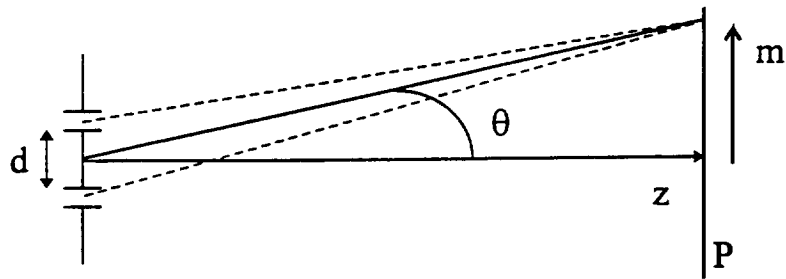


Figure 2.7 Young's Double Slit System

Maxima and minima of the interference pattern from the two slits in Figure 2.7 will be determined by Equation 2.66.

$$d \sin_m \theta = m\lambda \quad (2.66)$$

$m$  = order of the maxima

$\lambda$  = wavelength of the illuminating source.

### 2.3.2 Spatial coherence of an array of slits

Using a far-field image plane where the propagation distance  $z \gg \frac{d^2}{\lambda}$ , the diffraction angle  $\theta$  determines the position of the localized maxima from the center of the slits' separation  $d$ . The slits resemble two separate sources in an aperture plane, emitting rays of equal intensity and wavelength. The difference between two waves propagating from these slits is characterized by a difference in path length and phase depending on ray direction and distance traveled. The Young's double slit system can be expanded to incorporate multiple slits that are equally illuminated, resembling a linear array of sources.

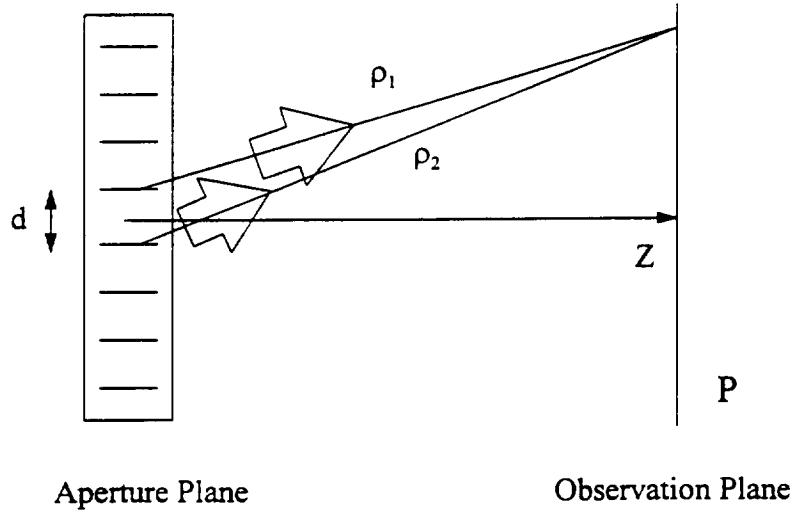


Figure 2.8 Multiple Slits for Young's Experiment

A quasi-monochromatic ( $\Delta\nu \ll \nu$ ) array is temporally coherent if the sources have a narrow linewidth. The linear array of slits in Figure 2.8 are sub-sources in a larger aperture for coherence analysis, as each slit is treated as a source for propagating beams contributing to a total wavefront. The spatial coherence of the emitted beams' wavefront is dependent on the correlation of the individual waves from the sources in the array.

This is described by the complex degree of spatial coherence,  $\gamma_{12}(0)$ , given for two beam paths  $\Omega_1$  and  $\Omega_2$  from source aperture points  $s_1$  and  $s_2$  respectively as:

$$\gamma_{12}(0) = \frac{\Gamma(\Omega_1, \Omega_2)}{\Gamma(\Omega_1, \Omega_1)} \quad 0 < \gamma_{12}(0) \leq 1 \quad (2.67)$$

(Marathay, 1982)

$\Omega_1$  and  $\Omega_2$  are two propagation paths from the source apertures to the observation plane, with zero time delay ( $\tau = 0$ ).  $\Gamma(\Omega_1, \Omega_1)$  is the self spatial coherence function for the ray path  $\Omega_1$ . The spatial coherence of these two waves is a comparison of their symmetry after traveling to the same plane P. The correlation of the waves at the observation plane is normalized to create the complex measure of spatial coherence,  $\gamma_{12}(0)$ .

This describes how closely a wave leaving the aperture from  $s_1$  resembles a wave leaving  $s_2$  after propagating to the same plane. The normalization is done with the self coherence function  $\Gamma(\Omega_1, \Omega_1, 0)$ , which compares the wave to itself with zero time delay. A spatially coherent beam from a synthetic aperture array of illuminated slits will have  $\gamma_{12}(0) = 1$  across the entire beam. With this set of conditions, any two initial aperture points will be spatially coherent at the observation plane.

### 2.3.3 Van Cittert - Zernike Theorem

Measuring the coherence at an observation plane locates the positions where phase differences from the source aperture are from piston errors, and to what extent the phase differences make the beam incoherent. Using the Van Cittert - Zernike theorem (Marathay, 1982), the spatial coherence can be described as the two-dimensional spatial Fourier transform of the optical intensity distribution from the source aperture  $A$ :

$$\Gamma(\rho_1, \rho_2, 0) = \frac{e^{ik(r_1 - r_2)}}{\pi Z^2} \iint_A \Gamma(s, s, 0) e^{-i2\pi \frac{x_{12}x_s + y_{12}y_s}{\lambda z}} dx_s dy_s \quad (2.68)$$

(Marathay, 1982)

$\Gamma(s, s, 0)$  describes the optical intensity function at the aperture,  $A$ , for the vector

coordinate  $s$ . The separation between planes is  $z$ , and the propagation distances  $f_1$  and  $f_2$  (see Figure 2.6) are from the center of the aperture to positions  $(x_1, y_1)$ , and  $(x_2, y_2)$  in the observation plane. The propagation paths are  $\rho_1$  and  $\rho_2$ . Coordinates for  $s$  in  $A$  are  $(x_s, y_s)$ , and  $\lambda$  is the mean wavelength of the quasi-monochromatic source.

Spatial coherence for multiple sources in a synthetic aperture can be optimized if the OPD of the traveling waves can be corrected for phase errors in propagation. To demonstrate an example of how spatial coherence and phase can be measured, let an aperture of  $N$  sources have a complex degree of spatial coherence given by  $\gamma_{N,N+1}(0)$  for any two sources in the aperture. This would give the complex degree of spatial coherence for source 1 and 2  $\gamma_{1,2}(0)$ , and  $\gamma_{3,4}(0)$  for sources 3 and 4. This can represent all of the spatial coherences of the sources through all the elements in an array in a summation :

$$\sum_{q=1}^N \gamma_{q, (q+1)}(0) = \Xi \quad 0 < \Xi \leq N \quad (2.69)$$

For this equation,  $\Xi$  is the determinate of the spatial coherence of the synthetic aperture. If  $\Xi$  is equal to the number of sources in the aperture, then the beam is coherent. If  $\Xi$  is less than the total number of sources, phase corrections must be made to some contributing beams in the aperture. For each  $\gamma_q(0) \neq 1$ , the  $q$ th beam can be corrected so that  $\gamma_q(0) = 1$  for all sources in the array. A phase profile of the synthetic aperture's beam can be calculated using this method, with  $\Xi$  values for each wave in the beam characterizing its contribution to the degree of spatial coherence for each source.

## 2.4 Fiber Theory

Fiber optic wave guides are commonly used to direct light from one location to another, transporting a signal inside the fiber instead of propagating through air. Fibers can eliminate the need for directional optics as it guides the light, and they can perform some operations not possible with conventional free-space propagation. The path of light through a fiber can be described with ray optics using a plane wave of the form  $Ae^{i(kr-\omega t)}$ . This assumes that  $r$  is along the direction of propagation, and  $k$  is the wave number for light.  $A$  is the amplitude of the wavefront.

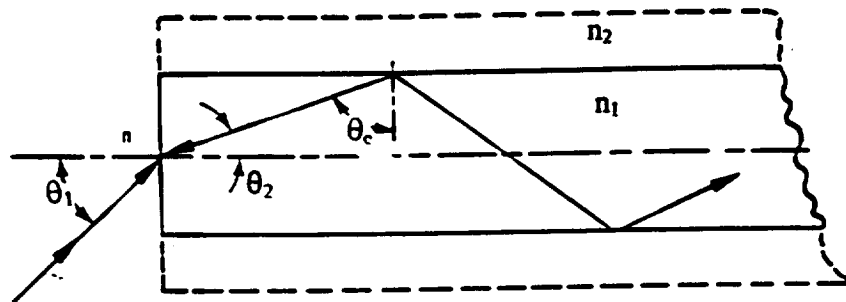
Knowing Snell's law of refraction for the boundary of two different media with indices of refraction  $n_1$  and  $n_2$ , interaction at the fiber interface is given as:

$$n_1 \sin \theta_1 = n_2 \sin \theta_2 \quad (2.70)$$

$\theta_1$  = incident angle in index  $n_1$

$\theta_2$  = refracted angle in index  $n_2$

For a ray of light incident on an optical fiber with angle  $\theta_1$ , it will continue into the second index at a refracted angle determined by Snell's law. This is shown in figure 2.9 for a step index fiber. Once inside the fiber, the ray will obey Snell's law and a condition called Total Internal Reflection (TIR) to continue moving along the length of the fiber. The cladding surrounds the core of the fiber, consisting of a third media of refractive index less than the fiber core, creating a condition where the light will reflect off of the interface if the angle of incidence is beyond the critical angle. This critical angle,  $\theta_c$  is given by:



(Krohn, 1992)

Figure 2.9 Fiber Launch and TIR



$$\theta_c = \sin^{-1} (n_2/n_1) \quad (2.71)$$

$n_1$  = index of refraction of fiber core

$n_2$  = index of refraction of fiber cladding

The rays that are incident at the critical angle and larger will reflect rather than refract at the surface interface. Step index fibers have a cladding that is very important to TIR, since it is used for beam propagation via TIR down the fiber. Step index fibers usually have a core of glass (fused silica is most common), with materials chosen based on the operating wavelength, especially for single mode fibers. The conditions for TIR are set up with the initial injection of light into the fiber. An acceptance cone of rays using the critical angle of the fiber determines which entry angles may propagate down the fiber and which will leak out and escape through the cladding layer. Equation 2.72 is the numerical aperture of the fiber if it is in air.

$$\sin \theta_c = \sqrt{[n_{\text{core}}^2 - n_{\text{cladding}}^2]} \quad (2.72)$$

Modes of a fiber are the individual waves that are allowed to propagate down a fiber of fixed diameter and core index. The number of allowed modes is defined by the V number for a fiber, (Krohn, 1992) given as Equation 2.73 for a particular radius and indices of the core and cladding.

$$V = \frac{2\pi}{\lambda} a n_1 \sqrt{2\Delta} \quad (2.73)$$

$a$  = core radius       $n_2$  = index of the cladding

$$n_1 = \text{index of core} \quad \Delta = \frac{n_1^2 - n_2^2}{2n_1^2} \quad (\text{Udd, 1991})$$

Single mode step index fiber has a smaller core diameter than multi-mode fibers, with single mode fibers allowing only one mode or propagating wave, to travel down the length of the fiber. The incident angle on a single mode fiber is very exact, with alignment of such a fiber needing very accurate positioning for maximum throughput of light. Multi-mode fiber will usually have a  $V^{\#}$  number much greater than 2.5, with the single mode cutoff below about 2.4. Other fiber types have a change in the index of the fiber core with radius. Gradient index fiber has a tapering index with radius, allowing a lower number of modes and less spreading of pulses in a propagating wave train.

For polarization sensitive systems, polarization maintaining (PM) fiber can be used to maintain linearly polarized light during propagation down the fiber.

Manufacturing processes that alter standard circular core are used create PM fiber.

Elliptical core fibers or stressors placed in the fiber creates birefringence to propagate linearly polarized light. Various PM fiber structures are shown in Figure 2.10.

## 2.5 Fiber interferometers and sensors

Fiber optic interferometers are often used as sensing devices, as the optical phase of the light passing through the fiber can be modulated by stresses and other physical affects. The phase change is detected interferometrically by comparing the signal path to a reference path. The output intensity is modulated by a change in phase ( $\Delta\phi$ ) seen as a piston error of the signal arm fiber path with respect to the reference arm fiber path.

Fiber sensors are very sensitive, with detectable displacement values as low as  $10^{-13}$  meters. (Krohn, 1992) There is also very low light loss in fibers, since the beam

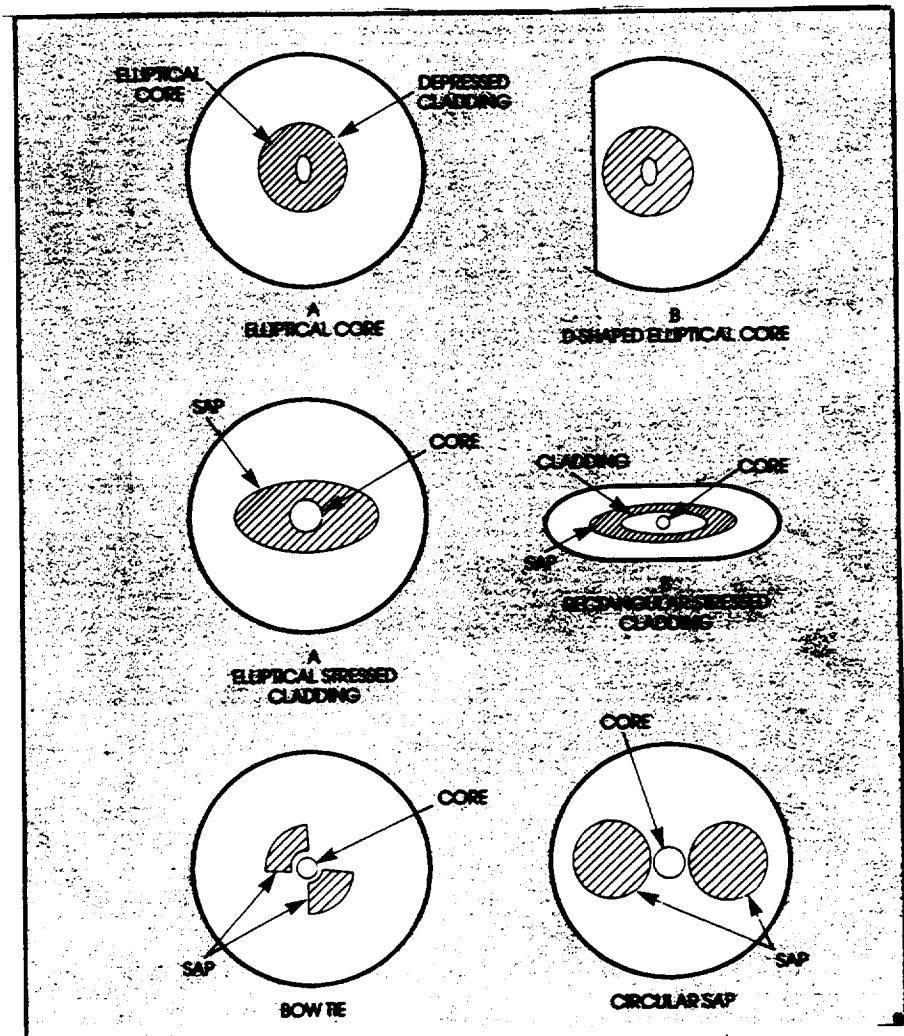


Figure 2.10 Polarization Maintaining Fiber Structures

(Fiber Optic Trends, 1988)

attenuation is low for carefully chosen optical sources. Stretching or squeezing the fiber will change the length of the fiber or some other characteristic of the core that affects the optical signal.

Fibers may also be stretched to maintain a specific OPD. The most common form of fiber stretchers are piezo electric devices that expand or contract when an electric current passes through them. They are often made of lead-zirconate-titanate (PZT). (Udd, 1991; Kingsley, 1978) Piezo electric phase modulators stretch fiber to change their length and OPD. PZT-5A can be made into rings or wafers and are the most common forms of fiber optic phase modulators. Sending a signal voltage across the PZT material changes its size, thus mechanically stretching fiber that is wrapped around it. These phase modulators are usually operated at some modulation frequency. PZT devices have acoustic resonances which are very important to frequency response. They are very sensitive to input voltage when operated on resonance. PZT based modulators will have more expansion on resonance, and can expand non-linearly. Resonant frequencies are determined by device geometry, piezo electric material type and mode of operation. (Udd, 1991; Kingsley, 1978) Bending and stretching the fiber induces a birefringence in the stressed region, changing the polarization properties of the fiber. This is often why PM fiber is used in systems that use a piezo electric phase modulator.

Stretching the fiber creates a change in OPD that is seen as a phase shift when compared to a reference path. This is usually observed with interferometry. Stretching optical fiber creates two types of phase delay, integral and differential. The integral phase delay is caused by light traveling through added path length,  $\Delta L$ , and is measured using

an external reference path. Integral delay is much greater than the differential phase delay. The differential phase delay is caused by an index change in the core,  $\Delta n$ , and the birefringence in the fiber. (Martini, 1987) Winding fiber around a cylindrical phase modulator, like a PZT ring, causes stress induced birefringent effects from the bending process. (Kingslake, 1978; Yoshino et al., 1982). Equation 2.74 shows how phase changes for a fiber of length  $L$  stretched by an amount  $\Delta L$ .

$$\phi(\Delta L) = k [L \Delta n + n \Delta L] \quad (2.74)$$

$k$  = wave number                       $\Delta n$  = photo-elastic effect induced index change

$n$  = core index of refraction       $\Delta L$  = change in fiber length

$L$  = length of stretched fiber

(Yoshino et al., 1982; Bergh 1983; Krohn 1992)

Stretching the fiber will change the length,  $\Delta L$ , and the refractive index,  $\Delta n$ , from a photo-elastic effect. The difference in path length between the arms in a two path fiber interferometer needs to be less than the coherence length of the laser source. If this is violated, the interference fringes will not have good visibility, since wavefronts from different wave trains will not interfere well. (Born and Wolf, 1975) Fiber interferometers are set up as single beam (Fabry-Perot, Sagnac ring) or two beam (Twyman Green, Mach-Zehnder) systems. Heterodyne systems use electronics and an acousto-optic cell to change the operating frequency for sensing and detection, while homodyne systems are very polarization sensitive and often require PM fiber, especially to avoid birefringence caused by mechanically stretching the fiber. (Yoshino et al., 1982) Sample fiber interferometers are shown in Figures 2.11 - 2.13.

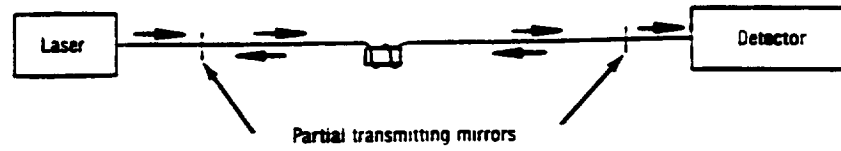


Figure 2.11 Fiber Fabry - Perot Interferometer

(Krohn, 1992)

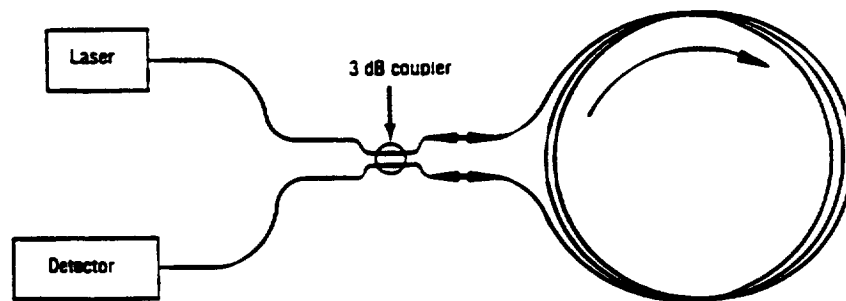


Figure 2.12 Fiber Sagnac Interferometer

(Krohn, 1992)

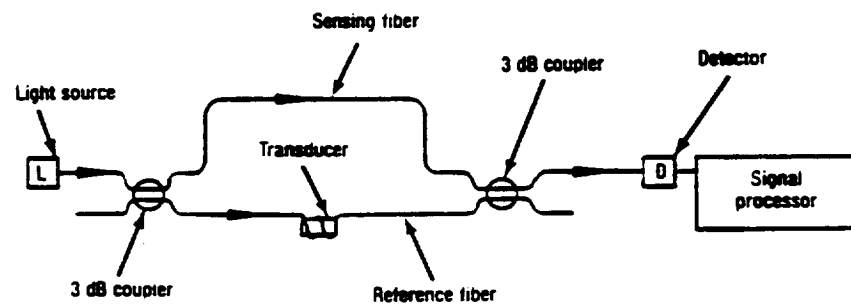


Figure 2.13 Fiber Mach - Zehnder Interferometer

(Krohn, 1992)

Sensor detection can decrease the intensity output due to destructive interference.

If the phase difference  $\Delta\phi$  is an odd multiple of  $\pi$ , then there will be an interference minimum, resulting in a dark fringe or minimum output intensity.

Modulation from maximum to minimum intensity is defined again by Equation 2.75. The change in output intensity of a fiber interferometer is shown in Figure 2.15, which demonstrates the dependence of  $(1 + \cos[\Delta\phi])$  (Krohn, 1992) as given in Equation 2.75.

$$I_{\text{final}} = \frac{I_{\text{initial}}}{2} (1 + \cos \Delta\phi) \quad (2.75)$$

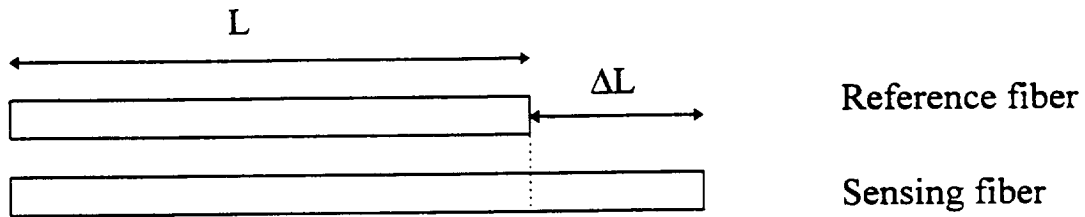


Figure 2.14 Sensing Fiber Interferometer and OPD

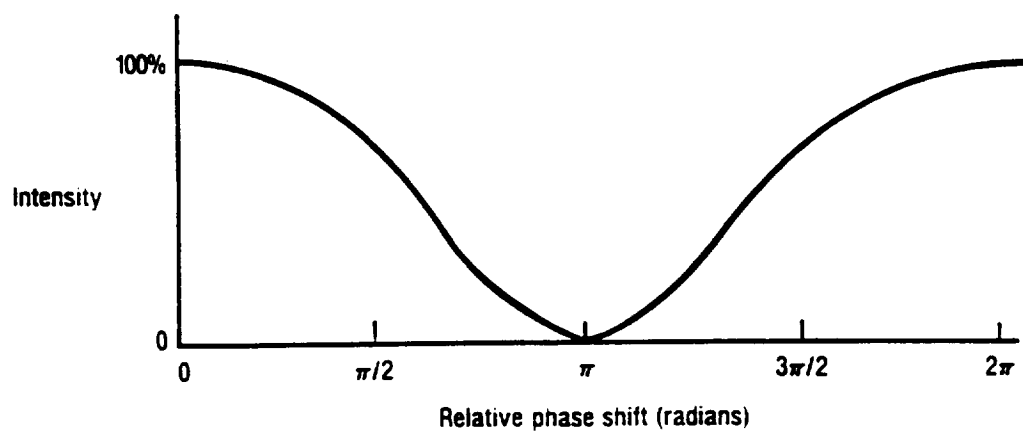
Both fiber arms have the same core index  $n$ , and operating wavelength  $\lambda$ .

From Figure 2.14 the reference and sensor phases are given by:

$$\phi = \frac{2\pi}{\lambda} nL \quad \text{Reference Phase} \quad (2.76)$$

$$\phi + \Delta\phi = \frac{2\pi}{\lambda} n(L + \Delta L) \quad \text{Sensor phase} \quad (2.77)$$

(Krohn, 1992)



Note: Sensitivity is a function of the slope of the intensity versus relative phase shift curve

(Krohn, 1992)

Figure 2.15 Phase shift and intensity in a fiber interferometer



The photo-elastic change of the index in the fiber,  $\Delta n$ , is incorporated into the  $\Delta L$  term. It is used in Equation 2.79 for  $\Delta\phi$  using the photo-elastic tensor values, Poisson's ratio, and the modulus of expansion for the core material. Tensor constants for optical materials characterize how the refractive index will change as a function of fiber stretch  $\Delta L$ . (Yoshino, 1982; Martini, 1987; Udd, 1991) The change in refractive index from photo-elastic effects,  $\Delta n$  is given by:

$$\Delta n = \frac{n^3}{2} \{(\rho_{11} + \rho_{12}) \nu_p - \rho_{12}\} \frac{\Delta L}{L} \quad (2.78)$$

$\rho_{11}, \rho_{12}$  = Photo-elastic tensor constants for the fiber core material

$\nu_p$  = Poisson's Ratio

$n$  = index of refraction of the fiber core (Yoshino, 1982)

Inserting Equation 2.78 for  $\Delta n$  into the basic phase shift expression in Equation 2.74 gives Equation 2.79 as the phase change for a fiber length change of  $\Delta L$ .

$$\Delta\phi = k n \Delta L \left[ 1 + \frac{n^2}{2} \left( \{\rho_{11} + \rho_{12}\} \nu_p - \rho_{12} \right) \right] \quad (2.79)$$

Stretching a fiber can be used to correct for phase differences as long as a reference path is available to compare path length and piston error. OPD modulation using a piezo electric fiber stretcher is one solution to phase mismatches in propagating beams since the stretch correct this.

## **CHAPTER III**

### **EXPERIMENT**

#### **3.1 Experiment Introduction**

The initial experimental work presented here began by reviewing the previous system used by NASA researchers. Analysis of its shortcomings pointed out a need for a new fiber-stretching device. After locating an appropriate piezo electric fiber stretching actuator, part one of the experiment began. This involved testing the piezo electric actuator with a fiber optic interferometer. The fiber stretcher is the key device in the system, and was characterized with a Mach-Zehnder interferometer and a He-Ne laser operating at  $\lambda=632.8$  nm. Part two of the experiment substituted the He-Ne laser with a Ti:Sapphire laser tuned to lock in the optical power amplifier, supplied by Phillips Labs at Kirtland Air Force Base. This interferometer system used different fiber and optics for the near IR source wavelength.

The experiment is relatively simple in theory. The path length of one arm of the fiber interferometer is changed by stretching it with a piezo electric actuator. The interference pattern creates fringes that will move when the fiber is stretched. Stretching the fiber creates a change in path length that is seen as a phase shift in the fringe pattern.

Phase modulation is calculated according to the fringes' movement and the drive signal to the fiber stretcher. The semiconductor optical amplifier boosts output power of the light coming through the stretched fiber arm while the phase is being changed.

### 3.2 Injection Locking Semiconductor Optical Amplifiers

The optical amplifier used in the experiment was an AlGaAs multiple quantum well device on loan from PL/LIDA division at Phillips Labs at Kirtland Air Force Base. It was the 10 emitter Techmo Demo design, two of which were sent to Marshall Space Flight Center for this work. A single mode Panda PM fiber couples into the amplifier that has ten channels operating at 860 nm when locked. One channel is used on the amplifier in the experiment so that the locked-in power amplification can be seen easier. The amplifier has a ridge waveguide y-branch to split the injected light into the ten channels. The light is guided through a phase modulator region on the chip, which is biased slightly to make it transparent. The light travels through the amplifier, which emits spontaneously from the excited region unless locked by the injected signal. The electrical ground for the device is the mounting heat sink, which had a lead running to the current source common ground line.

The device's temperature was controlled with a water cooled mounting block machined at NASA Marshall Space Flight Center Optics and RF division machine shop. The temperatures of the amplifier and block were measured with a thermocouple system and a Fluke multimeter. The sensitivity of the thermocouple monitored amplifier

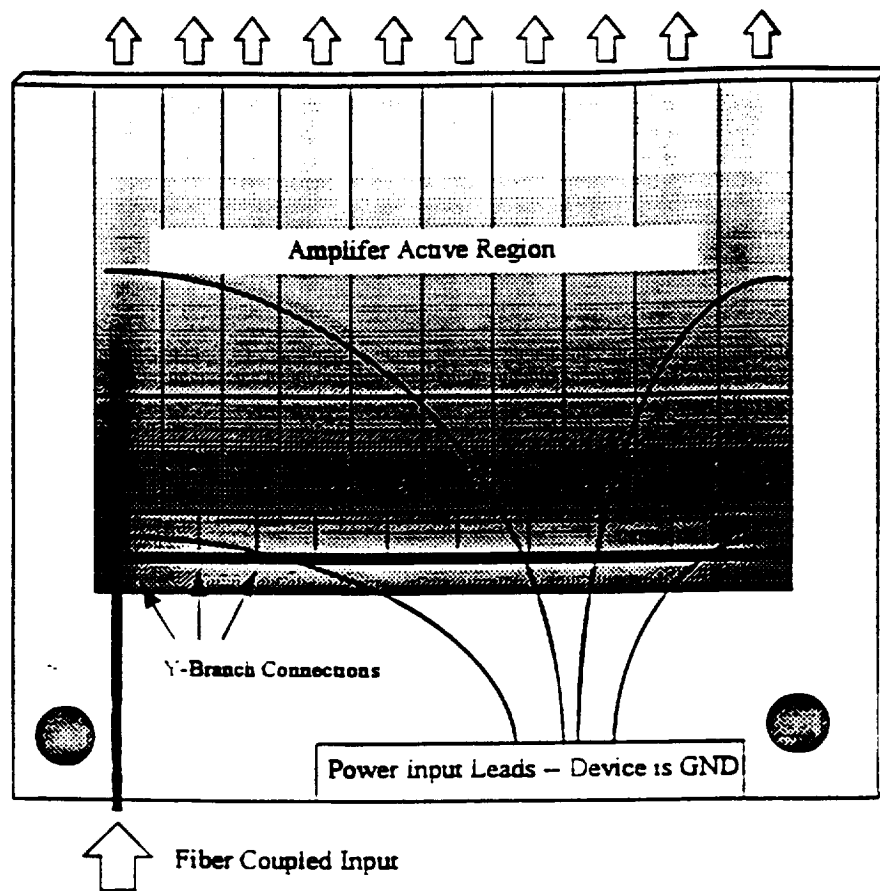


Figure 3.1 Injection Locked Semiconductor Optical Amplifier (ILA)

(Burke, 1996 submitted to Optics and Photonics News)

temperatures with  $\pm 0.1^\circ\text{C}$  error. The temperature of the amplifier was kept at or below  $60^\circ\text{F}$  ( $15.5^\circ\text{C}$ ) at full power as directed by the Phillips Laboratory's specifications. Temperature measurements were made from the thermocouple control box. The amplifier was also operated below  $15.5^\circ\text{C}$  in order to observe efficiency changes in the semiconductor device, since they tend to operate better when cooled. Figure 3.1 is a diagram of the amplifier with the injection fiber and power leads. (Burke et al., 1996) The amplifier is very similar to semiconductor diode lasers, except anti-reflection coatings replace a laser's mirrored end faces. Since it is a diode device, current limited sources were used to control output power.

Semiconductor optical amplifiers have been used for coherent coupling (Yariv and Usry, 1986), linear repeater systems (Yamamoto, 1980), receiver preamplifiers (Simon et al, 1983), and optical detectors (Ikeda, 1985). They have a large power output, and injection locking to a master oscillator generates a single mode operation. (Andrews, 1986) Injection locking an amplifier to another laser creates a pair of lasers which use the same optical frequency and longitudinal mode, allowing coherent coupling through phase modulation.

The output mode of an injection locked amplifier (ILA) is the same as the injected signal, with all other modes suppressed inside the active region of the device. (Kobayashi and Kimura, 1981) Data from Phillips Labs tests of the Techmo device in 1984 demonstrated amplification of the injected signal up to 30 dB in certain channels. These amplifiers preserve both the phase and mode of the injected beam, allowing a master oscillator and power amplifier (MOPA) system to be implemented for a high power

source with an array of ILAs. (Kwon et al, 1992) Coupling the output from two ILAs is a matter of correcting the phase difference of the two beams. This could then be expanded to use multiple sources in several arrays. This has been demonstrated in interferometric systems, with coupling efficiencies up to 97% for a two amplifier experiment. (Schuster and Andrews, 1992)

Table 3.1      Injection Locking Optical Amplifier Power Requirements

Device Number 446-78A Techmo Demo design

<u>Amplifier Component</u>	<u>Operating Current</u>
Amplifier Current	1.5 amperes
Y Branch Current	500 milliamps
Modulator Current (transparency threshold)	16-20 milliamps

Table 3.2 Amplifier Power Characteristics

Channel Data	1	2	3	4	5	6	7	8	9	10
Injection Locked Power (mw)	103.9	114.1	96.42	109.0	96.45	118.8	89.12	126.0	122.7	122.8
Un-locked Power (mw)	73.73	73.63	53.61	71.32	25.16	68.53	25.73	57.11	70.37	94.53
Injected Signal Power (mw)	1.51	2.32	2.31	2.36	2.07	2.22	1.68	3.01	2.52	9.97

**Operating wavelength:** 860 nm

**Amplifier Temperature:** 10°-16° C

**Courtesy of Phillips Labs PL/LIDA at Kirtland AFB, Albuquerque, New Mexico**

### 3.3 Fiber Based Mach Zehnder interferometer system

Two laser sources were used in the experiment. A Spectra-Physics 30 mW 632.8 nm He-Ne laser was used to measure fiber stretch as a function of drive signal. The visible source measurements made alignment, fiber launch, and troubleshooting easier. After the system optics were changed to use a near infrared source, an SDL 5422 diode laser was used, however its range in wavelength was tunable only  $\pm 5$  nm from its mean wavelength of 835 nm. This diode laser was replaced with a tunable Ti:Sapphire laser to better match the operating wavelength of the injection-locking amplifier. A Coherent Innova 300 Argon laser pumped 6 watts at 488 nm wavelength into a Coherent 899 Ti:Sapphire laser. This tunable system emits wavelengths from 790 nm to 920 nm, and was set to 860 nm after calibration with a spectrometer. The Ti:Sapphire laser produced 200 mW at 860 nm, which was decreased with Melles Griot neutral density filters so that the imaging CCD camera and the amplifier were not saturated.

The entire system was bolted onto a Modern Optics air-suspended optical table to minimize environmental vibrations. Non-polarizing beamsplitters for visible and near infrared wavelengths were from Newport Research Company and OptoSigma. All mirrors were from Newport, as were the stages and 20x microscope objectives used for launching and retrieving light from the fiber. Melles-Griot 20x beam expanders enlarged the beam size after the light was retrieved from the fiber. A JVC CCD camera with a Fujinon TV lens imaged the interference pattern on a Sony color monitor. Amplified power was measured with a Newport silicon photo-diode, with the output displayed on a Tektronix oscilloscope. The reference arm of the interferometer was three meters of 3M



single mode fiber for 633nm for the He-Ne test system, and three meters of 3M single mode 830 nm fiber for the final system. Other optics, shims, beam dumps and mounts were from the NASA Marshall Space Flight Center Optics and RF division Quantum Optics Lab.

### 3.4 Piezo-Electric fiber stretcher

The fiber stretcher used in the experiments was a piezo electric actuator which used two PZT wafers that expand when a voltage is sent across them. The manufacturer and model used was the Canadian Instrumentation and Research Limited (CIR) 915 Fiber Stretcher. This device came standard with 25 wraps of Panda PM fiber wrapped on it. The experiment needed more sensitive expansion and OPD modulation, therefore customized models were made for both the He-Ne visible and Ti:Sapphire near IR sources. Each actuator had five wraps of Andrew Corp elliptical core single mode PM fiber epoxied to the piezo wafers, with the rest of the 3 meters of fiber loosely coiled around the stretcher. (Burke, Optics and Photonics News 1996 submission) A servo board mounted directly on top of the plastic casing drove the piezo wafers. The actuator operated with a  $\pm 15$  volt DC power supply and a  $\pm 5$  volt DC drive signal to control the piezo wafer voltage.

The entire device was in a plastic mount, with the fiber wrapped around an oval loop in the center. Fiber optic actuators are used as phase modulators for gyroscopes (Udd, 1991; Kingsley, 1974; Krohn, 1992) telescope arrays (Weaver, 1988), and passive sensor systems like hydrophones (Lagakos, 1982; Kingsley 1974; Stowe, 1982).

Table 3.1 List of System Components

<u>Component</u>	<u>Manufacturer</u>
30 mW He-Ne Laser	Spectra-Physics
5422 150 mW diode laser	SDL Inc.
Collimating aspheric optic	Geltech
Nonpolarizing beam splitters	Newport, OptoSigma
Fiber optic stages and objectives	Newport
Polarization maintaining fiber	Andrew Corp.
Single mode fiber	3M
Innova Argon laser	Coherent
899 Ti:Sapphire ring laser	Coherent
Fiber stretcher	Canadian Instrumentation and Research Ltd. - 915
CCD camera	JVC
TV camera lens	Fujinon
Silicon detector	Newport 818-BB-40
Double oscilloscope	Tektronix TM504
Multimeter	Fluke model 46
Function generator	Philips PM5133
Closed-loop water chiller	
IR viewer	Electrophysics Corp. IRV 7100
25 volt triple power supply	Power Designs TP 343B
Semiconductor optical amplifier	McDonnell Douglas/ Phillips Labs

Their ability to accurately stretch fiber over very small ranges and also allow a large dynamic range makes them ideal for use in fiber interferometers. They are often used to keep a fiber sensor at a specific detection range, where the contrast of light and dark fringes is large. This is called a state of quadrature, where the slope of the input power versus the output power is the greatest. (Kingsley, 1974; Lagakos, 1982; Udd, 1991)

When a sensor is in quadrature, it is the most sensitive to environment changes. Phase modulators are used to keep this quadrature point throughout any thermal drifting or signal fading. Figure 3.2 includes a photo of the CIR 915 fiber stretcher from the manufacturer. (CIR Ltd., 1995)

The CIR 915 fiber stretcher used a Power Designs TP 343B triple output DC power supply for the servo board power and as an initial drive signal source. The drive signal was changed to a Philips PM5133 function generator for applying modulation frequencies to the fiber stretcher. A Tektronix TM 504 oscilloscope monitored the frequency of the function generator signal, and the servo board power voltage.

Measurements of the fringe displacement as a function of drive frequency were taken for a maximum  $\pm 5$  volts signal. Smaller drive signal amplitudes can be used for more precise fiber stretch, however there is little response below 1 volt. The fiber was changed for the Ti:Sapphire laser and the injection locking amplifier system. The actuator used five wraps of single mode 830 nm PM fiber to replace the 632.8 nm fiber, and operated with the same power and resonant frequencies of 1.45 kHz and 8 kHz.

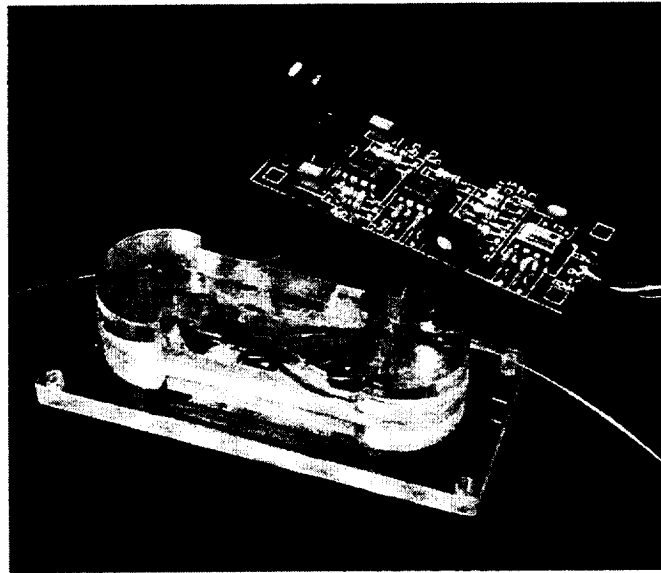
Table 3.4 Fiber Stretcher Specifications

<b>Piezo Electric Fiber Stretcher Components</b>	<b>Performance</b>
Power Designs TP 343B Triple Output DC Power Source	$\pm 15$ volts DC servo board power $\pm 5$ volts DC drive signal
Tektronix TM 504 Oscilloscope	Monitor servo board power and drive signal
Philips PM 5133 Function Generator	Create modulated drive signals from 0-10 kHz

### 3.5 Experimental Procedure

Initial work started with investigation of previous attempts toward phase modulation. Earlier research at NASA Marshall Space Flight Center's Optics and RF division developed the optimum array geometry for the amplifiers in a synthetic aperture. This was followed by a mathematical model of this aperture output for a phase-locked system of 1 and 2 rings of emitters. A sample of the work presented at a NASA presentation is included in Appendix A. The final results did not include the effects of random phases in the emitters, as shown in the Williams rectangular array model. (Williams, 1992)

The previous research did not finalize the choice of a fiber stretching actuator. Equipment from the SELENE program was borrowed to make a fiber stretcher, and a large actuator was built using three piezo electric columns to expand a pair of aluminum half-cylinders shown in Figure 3.2. (Montgomery, 1996) The clam-shell fiber stretcher had problems stretching the fiber since the fiber was not attached to the actuator, and there was only one wrap of fiber around the actuator.(Montgomery, 1996) This most likely led to the failure of the device. The earlier work concluded that it could not stretch the fiber enough in previous architectures. The clamshell actuator had the potential to stretch the fiber to create a change of 50 waves of OPD with only one turn of fiber and maximum power to the piezo columns. The clamshell device's flaw was in not attaching the fiber to the actuator to stretch it reliably and in controllable increments.



915 Piezo Modulator and Driver Card

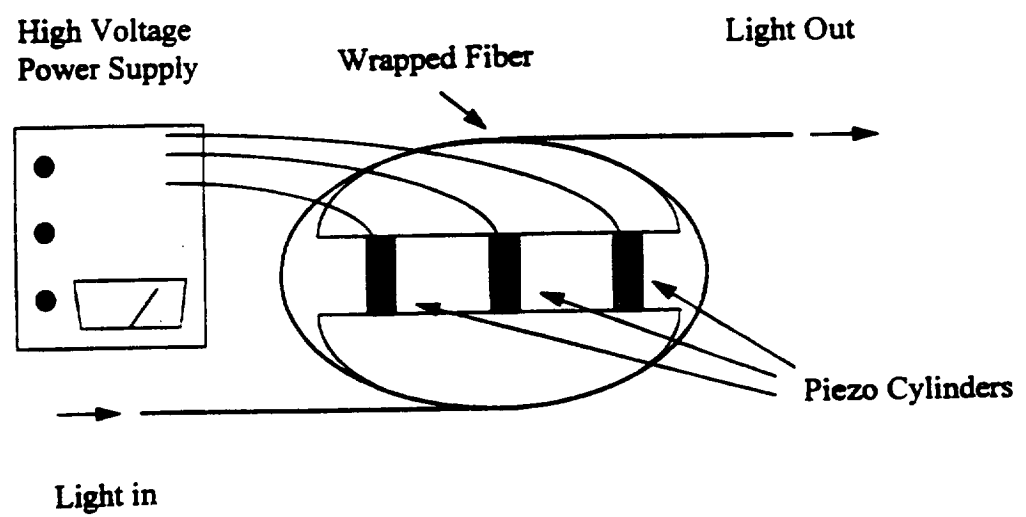


Figure 3.2 CIR 915 fiber stretcher and clamshell cylinder (NASA model)

### 3.5.1 Fiber stretcher test procedure

The CIR model 915 can stretch 5 wraps of fiber to create at least 2-3 waves OPD change accurately to a fraction of a wave of piston error using the driver card. This device was inserted into a Mach Zehnder fiber interferometer system to test the OPD change using a He-Ne laser. In the fiber stretcher test system, non-polarizing beamsplitters divided the laser beam into the two arms of the interferometer using vertically polarized light for maximum fringe contrast and visibility of the interference pattern. In each arm, the light passed through the beamsplitter and into the fiber launching stage, where a 20x microscope objective focused the beam into the fiber. A retrieval stage used another 20x microscope objective to collimate the emitted light from the fiber, and a beam expander allowed for better viewing and alignment of the interfered beams. A second non-polarizing beamsplitter combined the beams from the two paths to create an interference pattern. The sensing arm had the fiber stretcher and its length of fiber, single mode elliptical core PM fiber from Andrew Corp. The control arm had 3M standard single mode fiber for 633 nm. Each fiber arm was  $3.0 \pm 0.01$  meters long. The interfered beams were viewed with the CCD camera and monitor for fringe pattern location and alignment.

The actuator was tested for linear fiber stretch as a function of the drive signal, stretch accuracy, and total fiber stretch. This series of signal tests preceded insertion of the injection locking optical amplifier (ILA) and Ti:Sapphire laser. A sample data run of the fiber stretcher began with realignment of the interfering beams at the combining beamsplitter for maximum fringe contrast, aligning the fiber launchers for maximum light

throughput, and positioning the detector in the interference pattern. Next, the function generator was connected and set to the desired drive signal, and the oscilloscope displayed frequency and amplitude. The detector channel was connected and the oscilloscope was set to show both signals simultaneously. The silicon photodiode was used to measure the movement of the light and dark fringes across a stationary point. The piezo test system is shown in Figure 3.3 with the CCD camera and monitor used for alignment and initial pattern viewing. (Burke, 1996)

Several saw-tooth drive signals were used to test the fiber stretcher: a DC signal of 0-5 volts, modulated signals at 200 Hz, 1 kHz, 1.6 kHz, 4kHz, 8 kHz, and 10 kHz. Piezo wafer expansion per volt is the same for visible ( $\lambda=633$  nm) and near IR ( $\lambda=835$ nm , 860 nm) sources, therefore no problems exist when switching sources and fibers. The PZT wafers' expansion was not a function of the type of fiber used, but of the amplitude and frequency of the drive signal. The OPD change was a function of the core index, wavelength and fiber stretch.

### 3.5.2 Diode laser system

The actuator tests showed that it worked as expected, even exceeding NASA's required 1 kHz bandwidth. (Montgomery, 1996) The resonant frequencies were located and avoided so that the phase modulation would be linear with driver amplitude. The He-Ne source was replaced by a Spectra Diode Labs 5422 diode laser, a 150 mW source at 835 nm. The laser driver was an SDL 800 with a maximum output current of 1 Amp. Since the laser beam had a large divergence angle, and the saggital and tangential rays



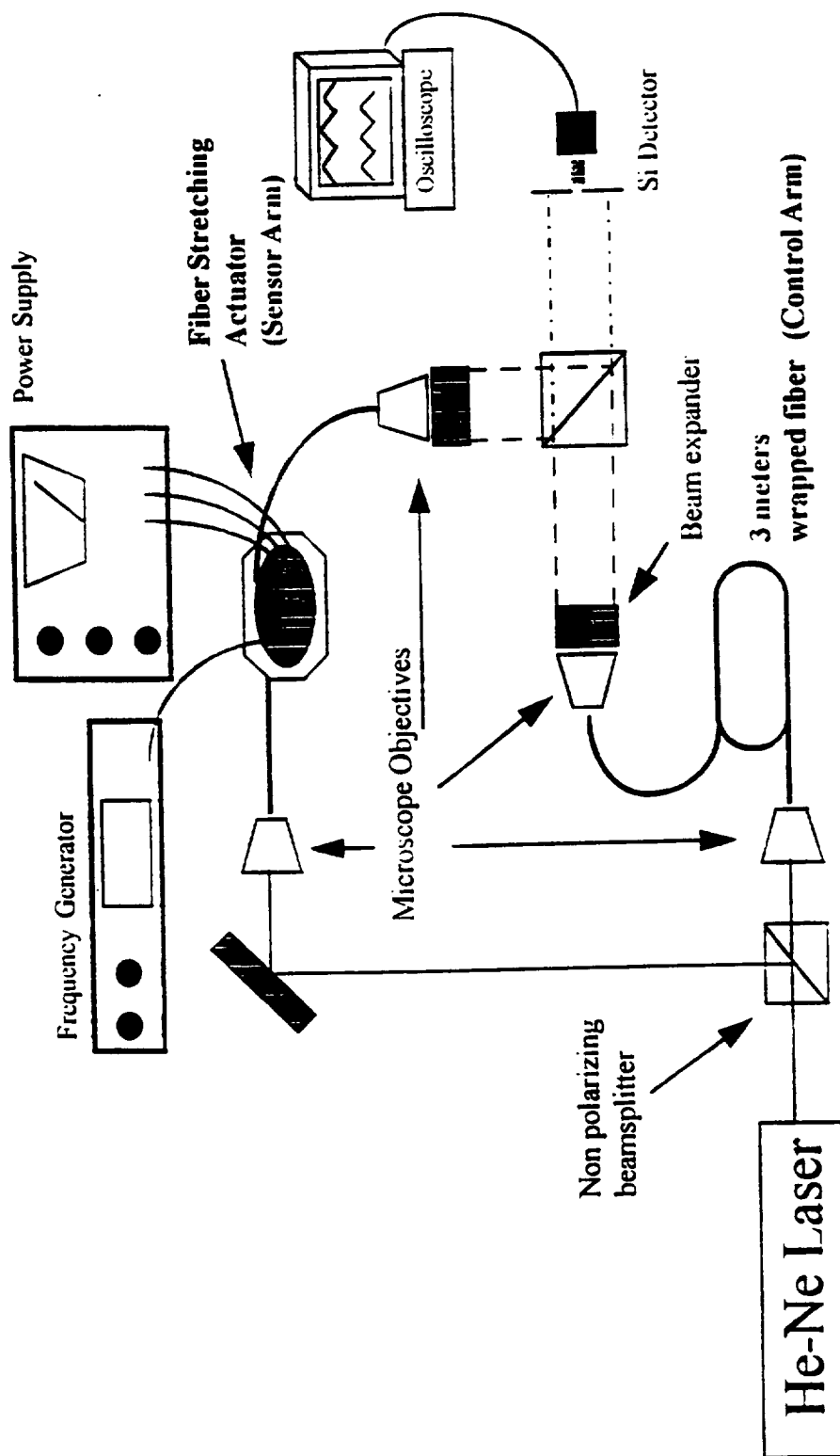


Figure 3.3 CIR Fiber Stretcher Test System

had different divergence angles, an aspheric optic was used to collimate the laser beam. A Thorlabs optic created a beam 2 mm in diameter at 100 mW output power with minimal divergence. The control arm's fiber was changed to 840 nm wavelength compatible fiber, and the fiber stretcher with 840 nm Andrew Corp fiber was inserted as the sensor arm. Linear polarizers were placed in front of the launching stages, and the axis of polarization was aligned to the sensor arm's PM fiber core to maximize the throughput. The system optics were changed for near IR wavelengths, replacing the visual wavelength optics. The beam from the sensor arm was focused into the fiber pigtail of the amplifier with a 20x microscope objective fiber launching stage, and the output from the biased transparent channel of the ILA was collected by the silicon photodiode.

### 3.5.3 Ti : Sapphire laser test system

The 860 nm optimum wavelength of the amplifier was too far away in wavelength from the 835 nm diode to observe gain from the injected signal using the diode laser as the master oscillator. When this laser could not be tuned to lock the amplifier, it was replaced by a tunable Coherent 899 Ti: Sapphire laser with an Argon ion pump laser. This would serve as a test MOPA system with the amplifier. The final system with the Ti: Sapphire laser is shown as Figure 3.4. (Burke, 1996)

The phase modulators on the amplifiers were biased with 16-20 mA to keep them from absorbing the injected signal. The optimal operating temperature of the device was 15.5 °C as given by Phillips Laboratories. The operation conditions for the amplifier are listed in Table 3.1. The amplifier's mounting block was used as a ground and heat sink,

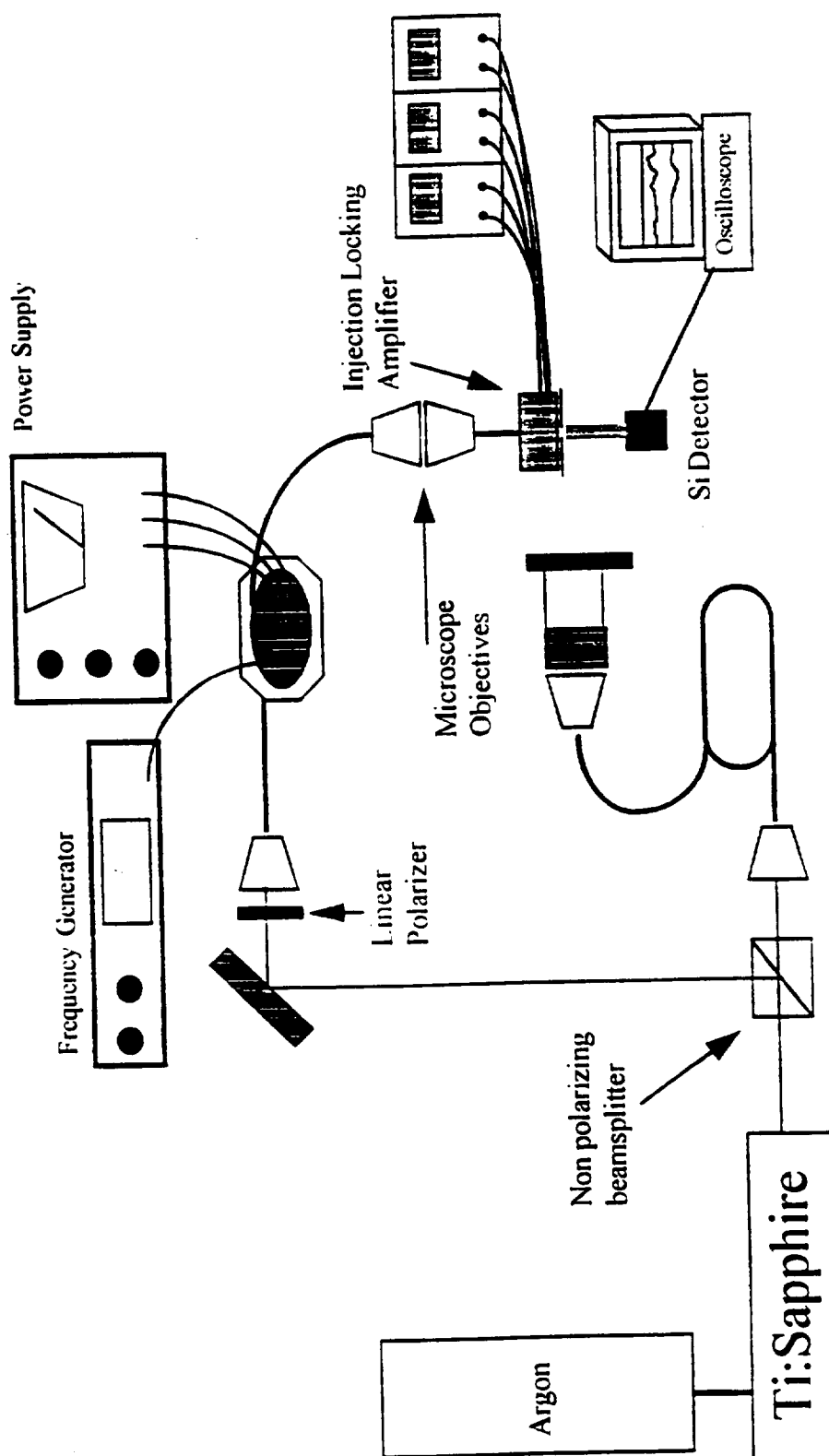


Figure 3.4 Ti:Sapphire laser and amplifier system for power measurements

and was cooled by a closed loop variable temperature water chiller. The coolant water was set to 10 °C to keep the amplifier and block at 15.5 °C when at full power, and was monitored by a thermocouple mounted underneath the amplifier device. Temperature tuning with this sort of device is primitive and coarse, so the coolant water was set at a constant temperature, and tuning for the amplifier was accomplished by changing the laser wavelength. The Ti: sapphire laser was the master oscillator in the MOPA.

The Ti: Sapphire laser was initially tuned to 860 nm. After 15-20 minutes the amplifier's temperature stabilized to 15.5 °C, during which the dominant output from the amplifier was spontaneous emission. The amplifier temperature was kept constant, so that the operating wavelength would not shift with environmental fluctuations. The laser's wavelength was adjusted with a micrometer on the Ti: Sapphire laser head to lock in the amplifier. Once the laser was tuned to the lock in wavelength, the amplifier's output power jumped from the spontaneous emission level on the oscilloscope. The amplifier's output power was detected by a silicon photodiode placed in front of the transparent amplifier channel. The output of the channels was blocked with a slit aperture on the exit face aligned to pass only the transparent biased channel.

After the amplifier was locked, the fiber stretcher's power was set to  $\pm 12$  volts DC, and the drive signal was connected to the actuator driver card from the function generator. The piezo wafer's expansion stretched the fiber and changed the OPD of the sensor arm in the interferometer, changing its phase with respect to the control arm. The amplifier and laser operating wavelength varied slightly from trial to trial, but remained near 860 nm  $\pm 5$  nm. Once the amplifier was locked and the laser wavelength recorded,

each trial used a 0-5 volt ramp signal to determine if the amplifier output changed from locked to unlocked operation.

### 3.6 Experimental Results

The piezo actuator test system showed the fiber stretch for various modulation frequencies was linear and within NASA's 1 kHz modulation bandwidth requirements for the power beaming phase correction system. The PZT wafers had two observable resonant frequencies at 1.45 kHz and at 8 kHz. These frequencies were not used for data and were not recommended for use since the wafers' response to applied voltage at these frequencies is not linear. A test of the fiber stretch at 8 kHz was made for information about the total PZT wafer expansion on resonance.

#### 3.6.1 Phase shift calculation

Using Equation 2.79 for the phase shift  $\Delta\phi$  ( $\Delta L$ ) as a function of fiber length and the tensor glass constants for a fused silica core, the PZT wafer induced phase change per applied volt can be determined using Equation 3.1.

$$\Delta\phi = kn(1 + \frac{n^2}{2} \{\rho_{11} + \rho_{12}\}v - \rho_{12}) \Delta L(V) \text{ radians/volt} \quad (3.1)$$

$\Delta L(V)$  = fiber stretch in microns per applied volt to PZT wafers

$$k = \frac{2\pi}{\lambda}$$

$\lambda$  = wavelength in microns (0.6328  $\mu\text{m}$ )

$$\rho_{11} = 0.120$$

$$\rho_{12} = 0.270$$

$$v = 0.17$$

(Yoshino et al, 1982)

$$n = 1.4616 \text{ for } \lambda = 0.6328 \mu\text{m} \text{ Andrew Corp fiber}$$

Equation 3.1 can be changed into an expression for fringe shift per micron of fiber stretch if the wavelength of the He-Ne laser is inserted in microns and the phase shift is given in number of fringes.

### 3.6.2 Mach - Zehnder interferometer phase shift

A Mach Zehnder interferometer is a single pass interferometer, as each fringe pair is a full wave of piston error, or  $2\pi$  radians. Equation 3.3 calculates fringe shift for any fiber length change  $\Delta L$ . The piston error created by changing the fiber length by  $\Delta L$  induces a phase shift given as Equation 3.4. The expansion of the PZT wafers and the fiber stretch is a function of signal to the wafers. Equations 3.2 - 3.4 are for 5 wraps of Andrew Corp PM fiber. A more universal equation for phase shift is given as Equation 3.5. This equation can be used to calculate phase shift for any actuator as a function of the PZT wafer expansion per volt per wrap of fiber.

$$\text{Fringe Shift} = \frac{1}{0.6328 \mu\text{m}} 1.4616 \left\{ 1 + \frac{1.4616^2}{2} (-0.20353) \right\} \Delta L(V) \quad (3.2)$$

(Yoshino et al., 1982)

$$\text{Fringe Shift} = 1.8076 \Delta L \text{ fringes/volt} \quad (\text{PZT response at 1 kHz}) \quad (3.3)$$

$$\Delta\phi = 2\pi(1.8076) \Delta L \text{ radians/volt} \quad (3.4)$$

$$= 11.357 \Delta L \text{ radians/volt}$$

$$\Delta\phi = 2.272 \Delta L \text{ radians/volt} \cdot \text{fiber turn} \quad (3.5)$$

### 3.6.3 Experiment Calculations

The experimental data was used to calculate the fiber stretch per volt for various modulation frequencies using Equation 3.3. Since the PZT wafers' expansion was linear to voltage, but frequency dependent, the modulation frequency was just as important as the signal voltage for the system calculations. The calculated PZT wafer expansion from the interferometer data is plotted against the modulation frequency of the drive signal in Figure 3.5. The graph would be flat if the PZT wafers had perfect expansion independent of drive frequency. The calculated phase shift with a 0-5 volt DC signal to the fiber stretcher is plotted as Figure 3.6. The calculated phase shift with a 5 volt amplitude and various modulation frequencies is graphed in Figure 3.7. These results are for the stretcher test system using 5 wraps of PM fiber for He-Ne lasers. The PM fiber core refractive index is 1.4616 for  $\lambda = 632.8 \text{ nm}$ , and 1.457 for  $\lambda = 840 \text{ nm}$ . Figures 3.8 - 3.13 are oscilloscope traces of the piezo test system's detector signal shown with the modulated drive signal displayed. Some of the figures have been enhanced for easier viewing. Figure 3.14 is the graphed data of the number of fringes that moved across the detector for various modulation frequencies.

### 3.6.4 Near IR system changes

An actual power beaming system would use a source with a wavelength close to 830 nm for optimum atmospheric transmission and ease of semiconductor manufacturing.

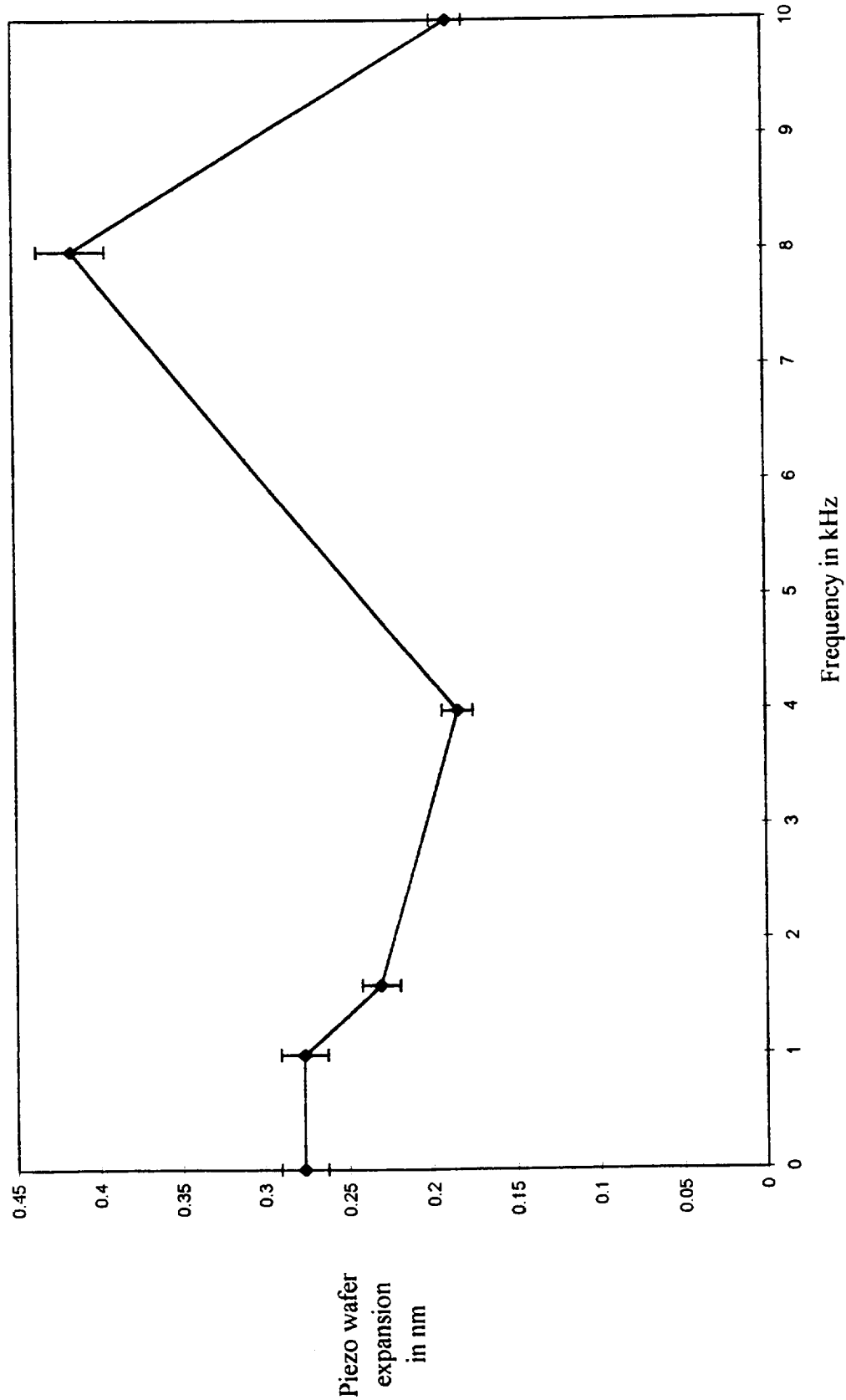


Figure 3.5 Piezo Wafer Expansion for test frequencies



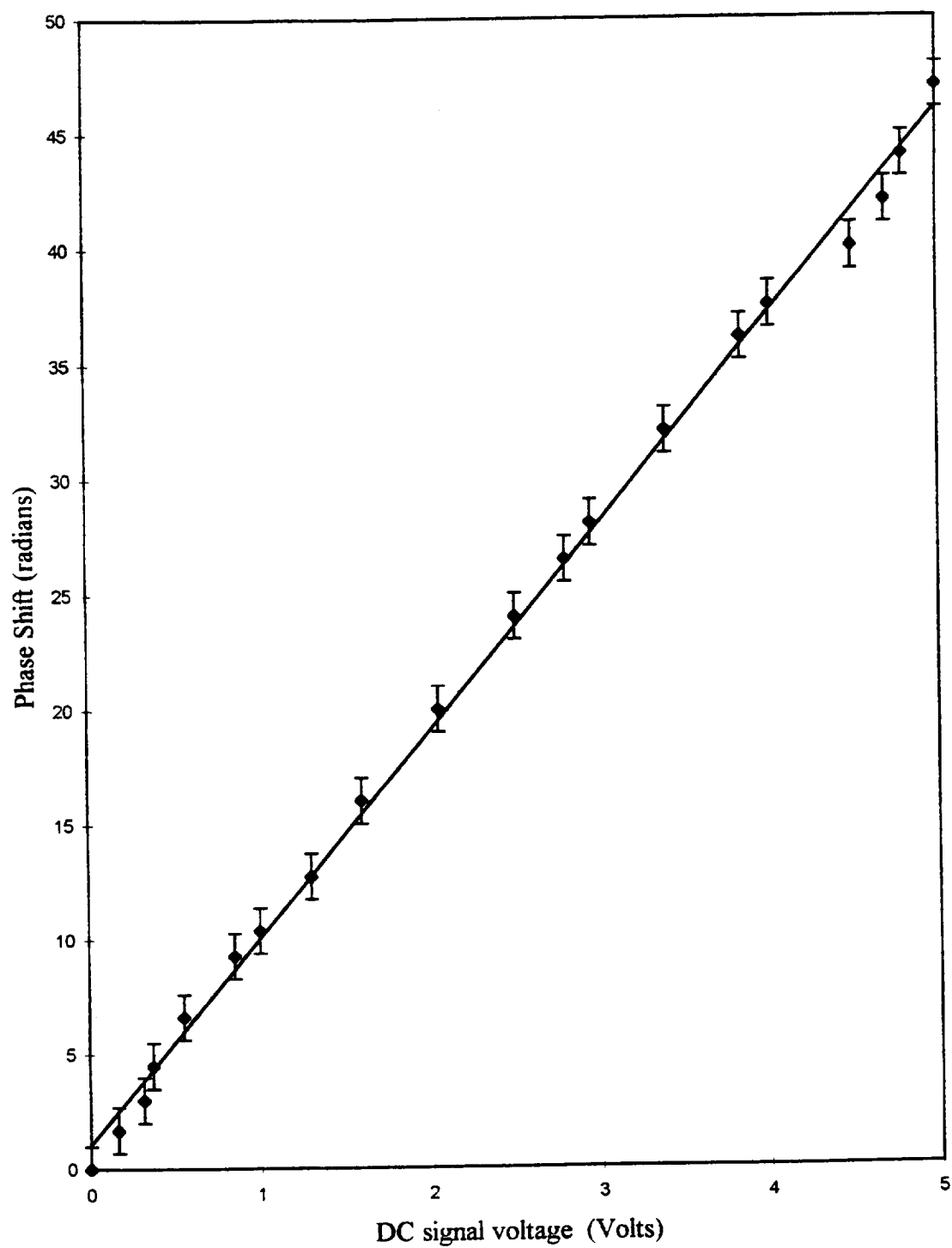


Figure 3.6 Fiber stretcher phase shift for 0-5 volts DC signal

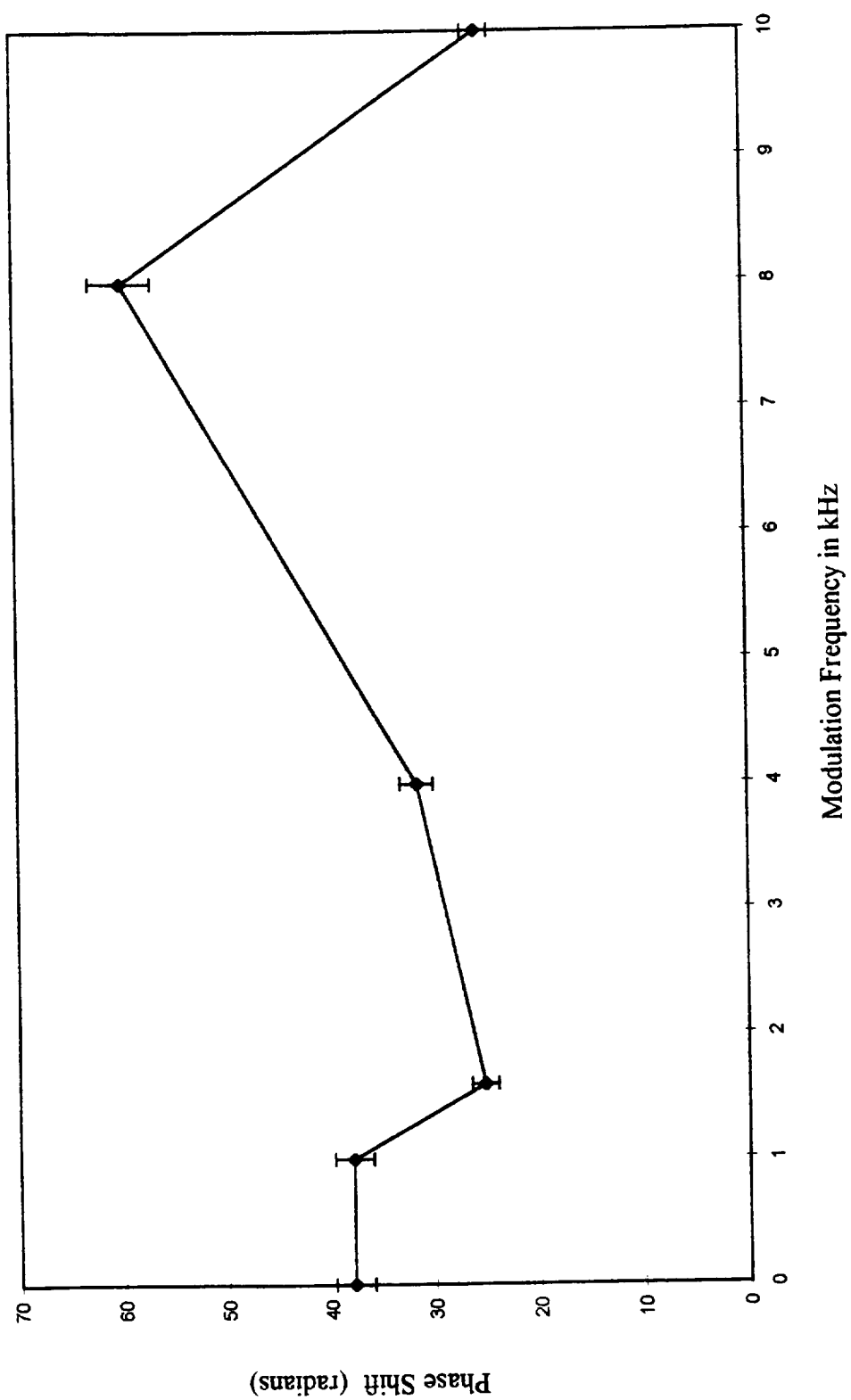


Figure 3.7 Phase shift for 5 volt amplitude with various frequencies

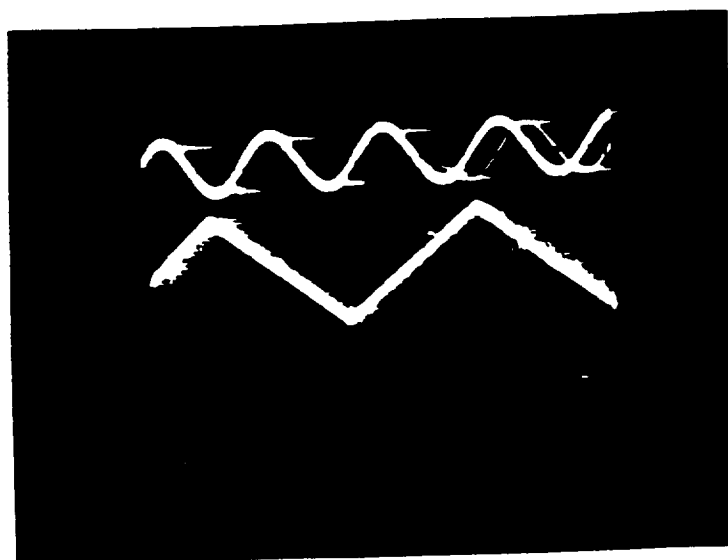


Figure 3.8 Oscilloscope trace for stretcher - 1kHz at 2 volts amplitude

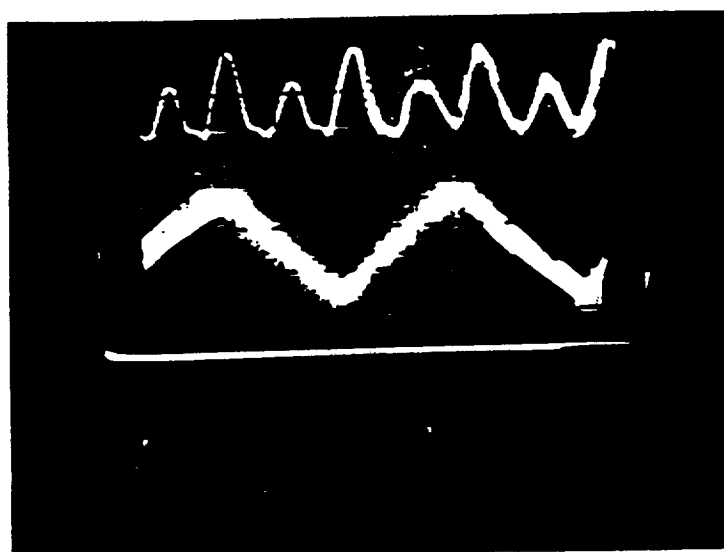


Figure 3.9 Oscilloscope trace for stretcher - 10 kHz at 5 volts amplitude

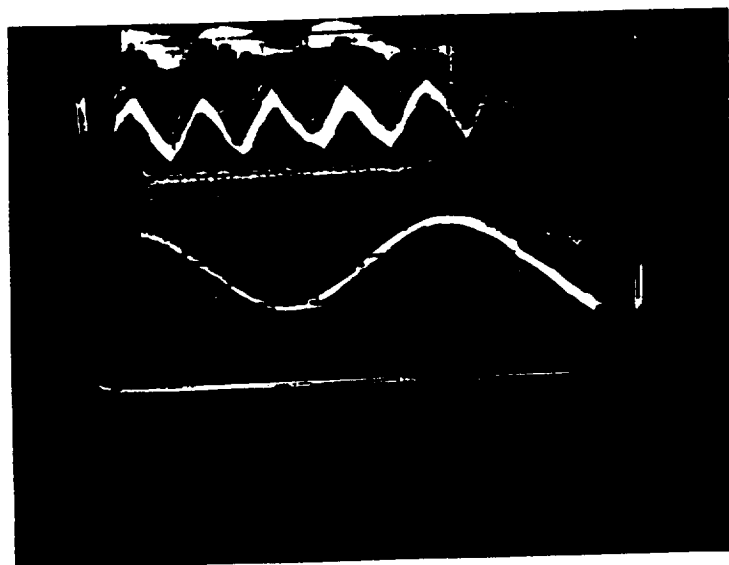


Figure 3.10 Oscilloscope trace for stretcher - 1.6 kHz at 5 volts amplitude

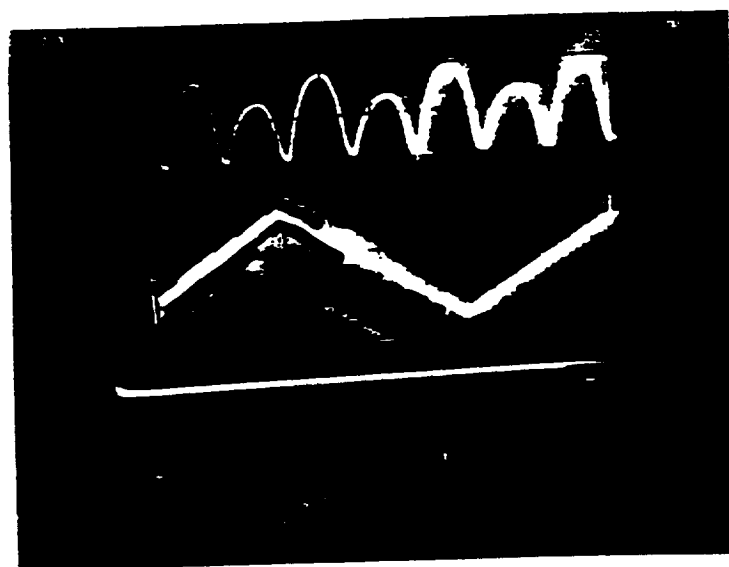


Figure 3.11 Oscilloscope trace for stretcher - 1 kHz at 5 volts amplitude

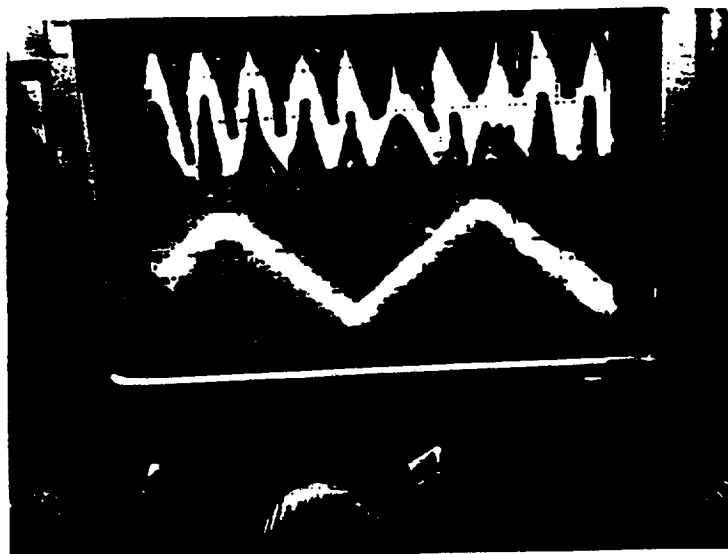


Figure 3.12 Oscilloscope trace for stretcher - 4 kHz at 5 volts amplitude

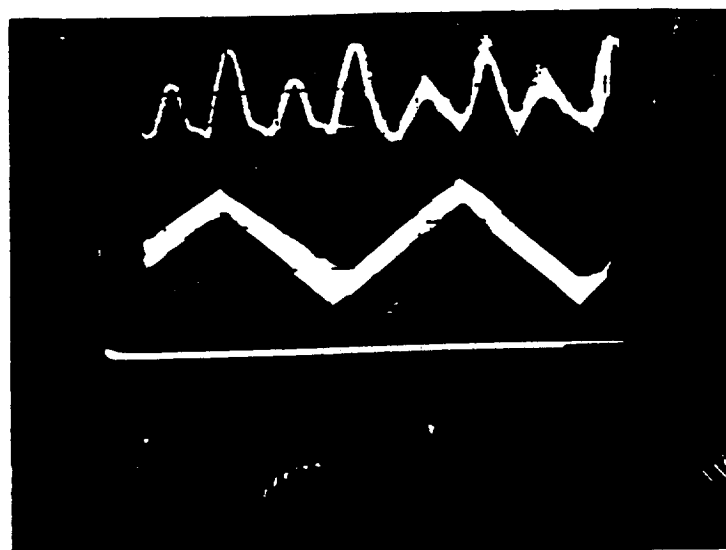


Figure 3.13 Oscilloscope trace for stretcher - 10 Hz at 2 volts amplitude

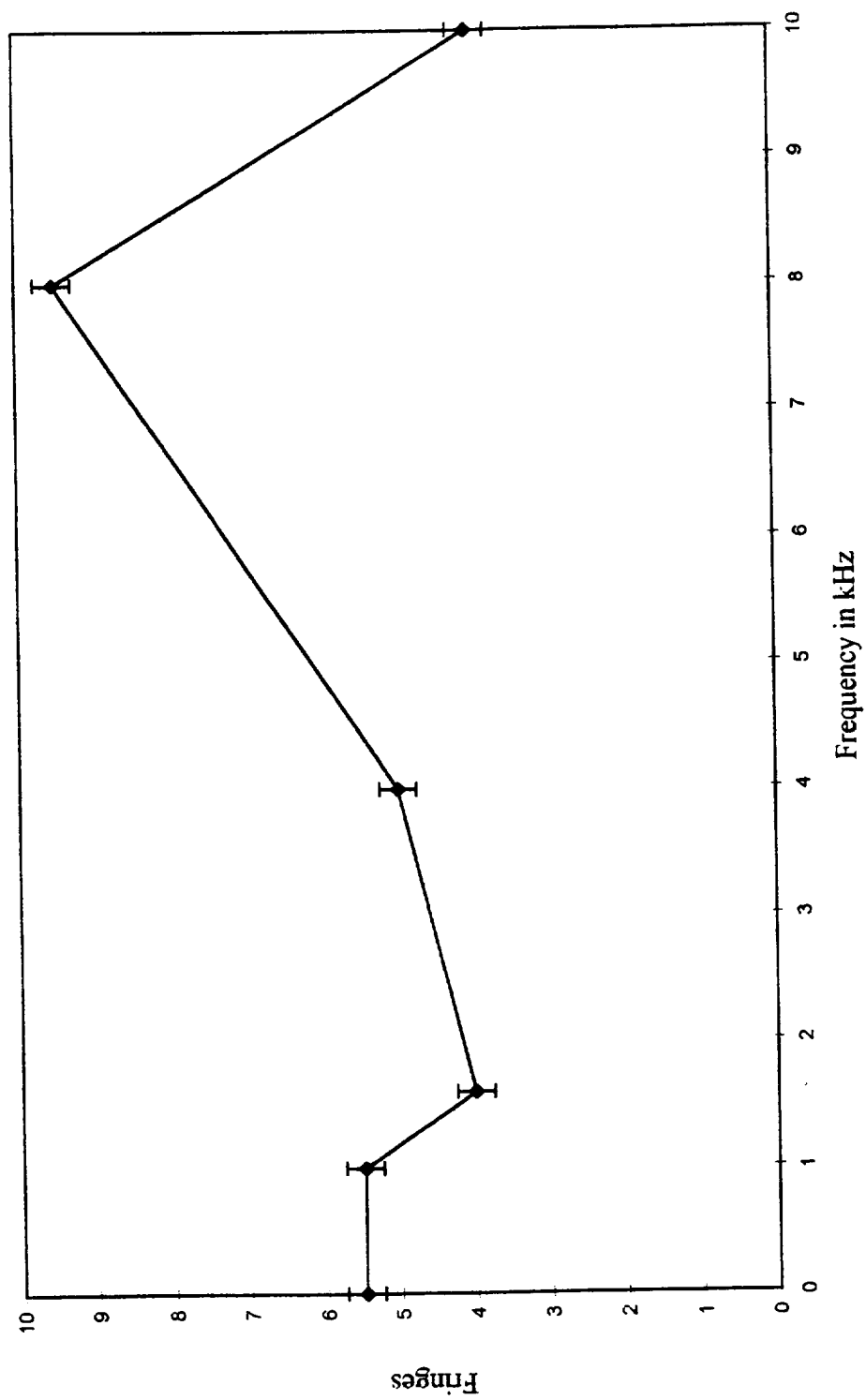


Figure 3.14 Fiber Stretcher Fringe Shift Versus Frequency

The adaptive optic system for this wavelength would have a different response than the He-Ne system using the same fiber stretcher since the fiber and laser would be changed. Equations 3.6-3.9 use Equation 3.2 and the index for PM fiber for  $\lambda=840$  nm and a  $\lambda=0.83$   $\mu\text{m}$  source for phase shift. Performance of the PZT wafers will not change for different fibers or lasers.

$$\text{Fringe Shift} = \frac{1}{0.83 \mu\text{m}} 1.457 \left\{ 1 + \frac{1.457^2}{2} (-0.20353) \right\} \Delta L(\text{V}) \quad (3.6)$$

$$\text{Fringe Shift} = 1.376 \Delta L \text{ fringes/volt} \quad (3.7)$$

$$\Delta\phi = 8.647 \Delta L \text{ radians/volt} \quad (3.8)$$

$$\Delta\phi = 1.729 \Delta L \text{ radians/volt} \cdot \text{fiber turn} \quad (3.9)$$

### 3.6.5 Amplifier output power

The output power increase for the optical amplifier was measured with the silicon detector and oscilloscope. The spontaneous, unlocked output of the amplifier channel was 53 mW at 1.5 A amplifier current and 200 mA y-branch current. This power came from channel number 3 on the amplifier. This channel was used since it operated the best of all the channels. Other channels were tested, but their output was more difficult to observe since they emitted more unlocked power. Most channels emitted around 70 mw when unlocked.

After tuning the laser wavelength to lock the amplifier, the output from the amplifier channel increased on the oscilloscope. The amplitude was 20 mV per division for the detector signal. Equation 3.10 converts the oscilloscope readings to incident

power using specifications from the 50 Ohm resistance silicon photo diode. The incident power is given as :

$$V = I R \quad \text{Ohm's Law}$$

$$I = V/R \quad \text{Amps} = \text{Volts} / \text{Ohm}$$

$$\text{Responsivity} = 0.6 \text{ Amps} / \text{Watt} @ 860 \text{ nm} = I / P_{\text{incident}}$$

$$\frac{1 \text{ Watts}}{0.6 \text{ Amp}} \left( \frac{V}{R} \right) = P_{\text{incident}}$$

$$\text{Detector impedance} = 50 \text{ Ohms} = R$$

$$P_{\text{incident}} = \left\{ \frac{1}{30} \text{ Watts} / \text{Volt} \right\} \{ V_{\text{oscilloscope}} \} \quad (3.10)$$

The oscilloscope measured 53 mW of spontaneous emission from channel 3 with 1.59 volts. The reading increased 60 mV when locked in, increasing the optical power by 2 mW. This was significantly lower than expected. This value should have been higher given the data in Table 3.2 for this amplifier. The power increase was tested with all channels, and the amplified power was the same or worse. It was impossible to see a power increase in the channels that had very high unlocked output power. The fiber stretcher's modulation frequencies used to test the amplifier lock were 200 Hz and 1 kHz.

The locked in amplifier did not change output power while the fiber was stretched. The performance of the amplifier was generally poor with or without a drive signal. The fiber stretcher's ability to modulate the phase of a laser beam was observed with the Mach - Zehnder system. The amplifier locked in the injection signal while the phase was changing in the sensor arm of the interferometer, but was not affected. The fiber stretcher changed the OPD at least 2 waves ( $4\pi$  radians) during injection lock as



well. Interferograms of the fiber stretcher test system are shown in Figures 3.15-3.20.

The figures are grabbed images of a moving fringe pattern, caused by changing the phase with the fiber stretcher. The images move too fast to see anything but a blur; however, when they are stopped, as they are in the figures, a good interference pattern remains intact. They are still shots of moving fringes, and some were enhanced for easier fringe viewing.

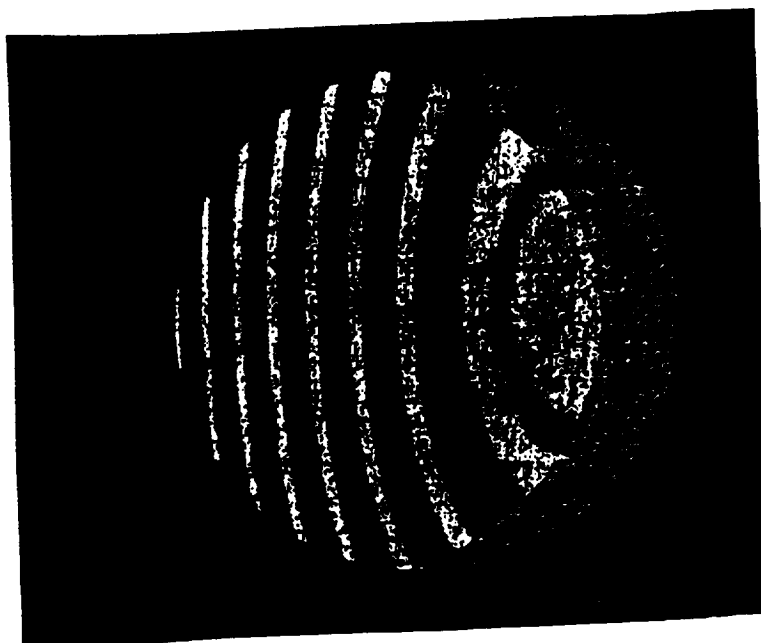


Figure 3.15 Fiber stretcher test interference pattern - 0 Hz

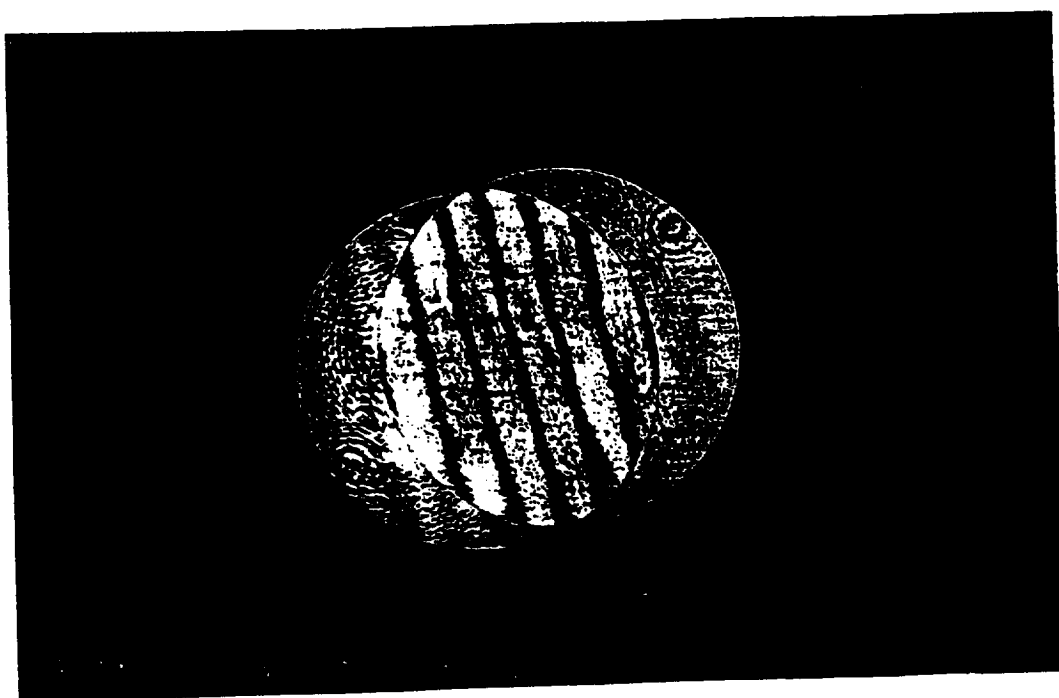


Figure 3.16 Fiber stretcher test interference pattern - 20 Hz

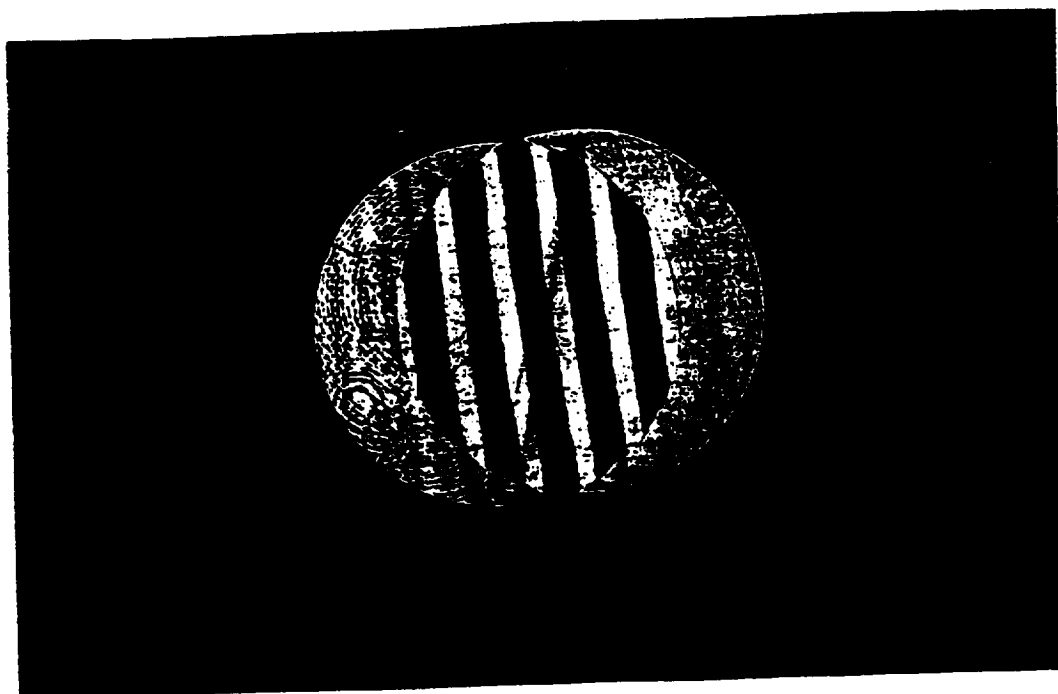


Figure 3.17 Fiber stretcher test interference pattern with extra shear

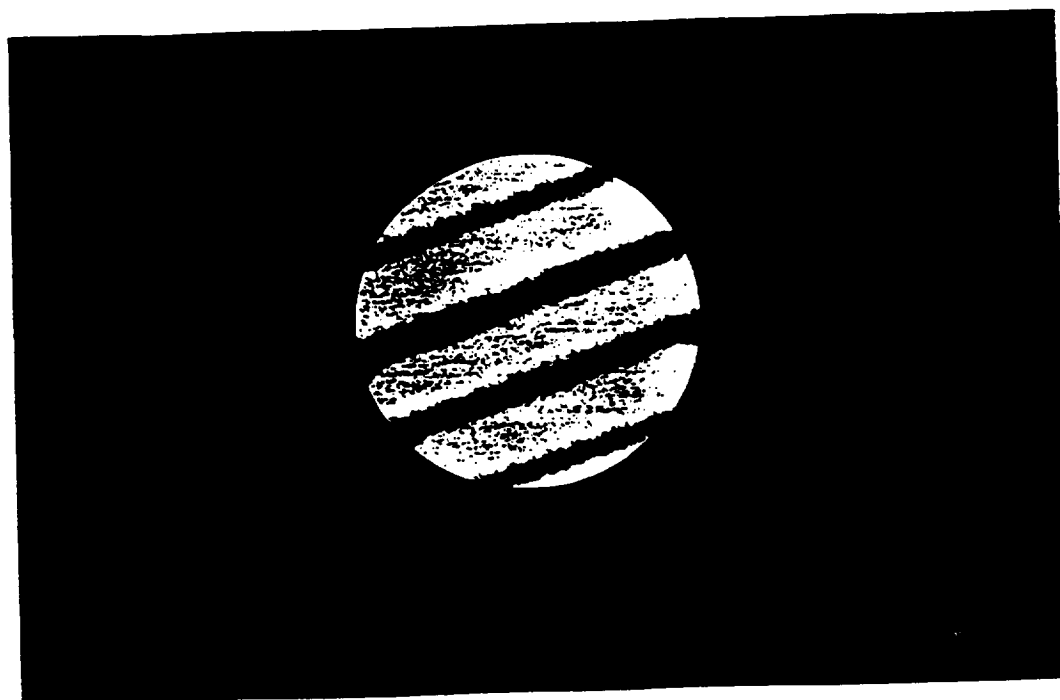


Figure 3.18 Fiber stretcher test interference pattern with tilt

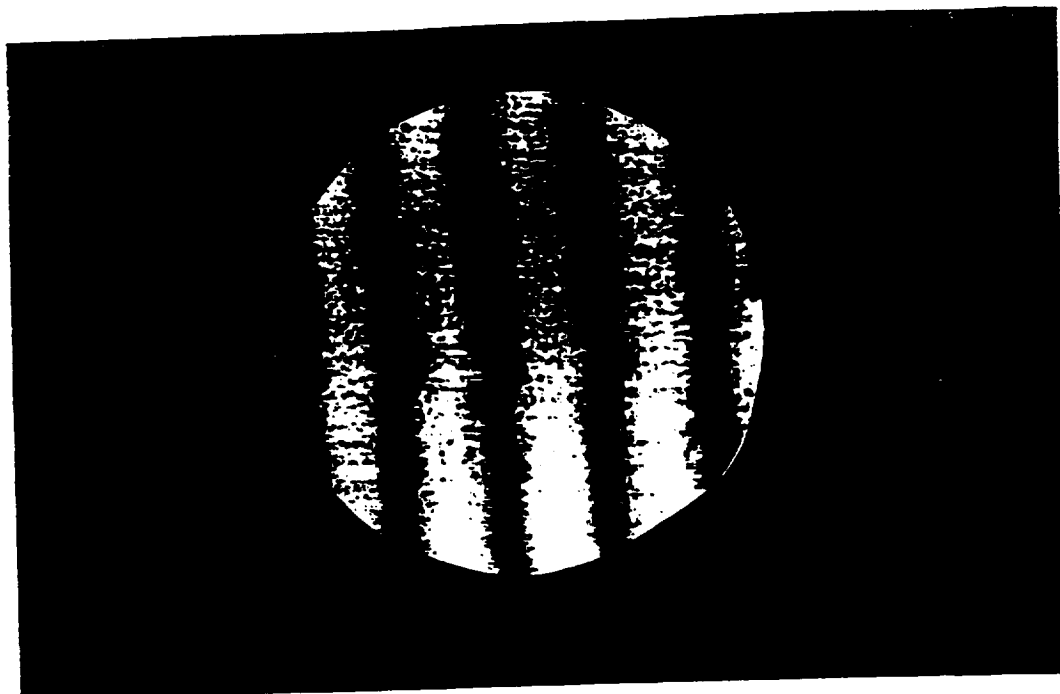


Figure 3.19 Fiber stretcher test interference pattern - 1kHz



Figure 3.20 Fiber stretcher test interference pattern - 200 Hz

## **CHAPTER IV**

### **DISCUSSION**

#### **4.1 System Considerations for Laser Power Beaming**

Laser power beaming can provide an option for space propulsion and vehicle onboard power, supplying laser power to future vehicles or current orbiting space vehicles. As of now, no efficient, reliable, cost-effective system exists to provide this laser power. Phased array power beaming may provide this power need with a synthetic aperture source. Individual sources in the array provide laser power on the order of watts, but a coherent sum of many sources can emit the on the order of kilowatts of laser power. A system to couple arrays of sources in a synthetic aperture would make a reliable and efficient laser source possible.

Coupling the power from arrays in a synthetic aperture onto a target requires a coherent beam of light. All sources must emit the same narrow linewidth for temporal coherence. Spatial coherence of a laser beam is dependent on the source aperture and phase of emitted beams from that aperture. Correcting phase differences in a beam with a very narrow linewidth can produce coherent propagating light. The correction process for a beam from an array must align the phase angles of all emitted rays in order to launch a coherent light beam onto a far field target. A master oscillator and power amplifier

system with a phase correction system could meet the temporal and spatial coherence requirements for space power beaming.

#### 4.2 Fiber Optic Phase Modulation

Using fiber optics and a Canadian Instrumentation and Research Ltd. model 915 fiber stretcher, the phase of one beam was changed over  $4\pi$  using OPD modulation. The induced piston error changed the phase of one beam traveling through the fiber stretcher with respect to a beam that just went through fiber. The piston error was created by changing the OPD in one arm of a Mach-Zehnder fiber interferometer with the 915 fiber stretcher. The other fiber arm was kept at a constant OPD, and served as a reference path length. The fiber stretcher could create OPD changes of over four waves with modulation frequencies from 0-10 kHz.

Fringe movement in the interference pattern indicated a phase shift caused by fiber OPD change when the actuator stretched the fiber. Phase correction can be monitored using a feedback system, performing corrections to the OPD using the fiber stretcher with up to a 10 kHz frequency.

In order to phase match beam paths across an array, the out of phase beams need a maximum  $\pi$  phase correction. This is a half-wave of induced piston error, which is easily attained with the CIR 915 fiber stretcher. Once the phase of a beam is sampled and corrected to a reference path in a feedback system, it can be amplified by an injection locking semiconductor amplifier which boosts the output intensity. An array of optical amplifiers with fiber coupled injection placed in a synthetic aperture geometry could

provide correctable, steerable, coherent power. Injection locked amplifiers that are locked-in to their source signal preserve the phase and mode of the injected beam, and can amplify the locking beam while the phase is changing. These tests and experiments demonstrated amplification of a laser beam from an injection locking optical amplifier loaned by Phillips Laboratories PL/LIDA group. The amplified emission from the amplifier was observed while the phase was changing in the sensor arm of the interferometer.

Investigation of a fiber optic phase modulator for an array of diode lasers has demonstrated that a fiber stretching actuator can correct phase differences in an array of sources. An array using a MOPA system with fiber stretchers in the fibers leading to the injection locking optical amplifiers can create a high power coherent beam. The phase of each emitted beam is correctable, and the semiconductor devices are reliable and efficient for supplying high power over a long lifetime. An array of sources is not likely to have total power shutdown, and small angle beam steering is possible using phasing across the array instead of using a steering mirror. These advantages make the MOPA system with fiber optic phase modulators a possible solution for a laser power beaming source.

### 4.3 Recommendations

Further research work would be beneficial in advancing the principles found from the investigation and results of this work. Customized, single channel, one-pass, multiple quantum well injection locking amplifiers need to be obtained to replicate an actual array emitter. Knowing the true dimension, power characteristics, and cooling requirements is crucial to effectively model the output from these devices. The Phillips Laboratory model amplifier was suitable for technology demonstration, but not for actual system characterization because of difficulty in locking in the amplifier and lower than expected amplification results. The new amplifier should be manufactured to amplify a 835 nm injected signal, since this is a very good wavelength for transmission through the atmosphere. It is a good choice for conversion efficiency with satellite photo-voltaic detectors, and ease of obtaining the master laser since 835 nm is a common diode laser wavelength.

Sensing electronics to fit a system for sensor fiber interferometers, such as a sampling Fabry-Perot interferometer, could incorporate feedback and correction to test the modulation frequency of the fiber stretcher with phase detection and correction at the target. This would also require fiber couplers and beamsplitter to be added into the amplifier fibers. Collimating optics such as lenslet arrays or small diffractive optics would provide high throughput and a collimated beam for test bench power measurements and far-field beam steering capabilities with a phased array of two or more amplifiers.

Feedback systems from the target could provide spot size and power distribution information usable by a feedback and correction loop at the source aperture itself.



Propagation distortions and beam misshaping caused by atmospheric conditions can be corrected with spatial light modulators, providing a method to test phase information from the target to correct piston errors and produce optimal spot size and power.

These additions to the current system and further research would facilitate progress towards system characterization with scaled down system modeling and bench testing. Completion of a system this size requires comprehensive technical and experimental test data, both of which would be greatly improved by adding these recommendations to the current system and continuing the scope of research.

#### 4.4 Conclusion

The results of from this investigation conclude that a piezo electric fiber stretcher can reliably serve as a phase modulator. The CIR 915 fiber stretcher used in this experiment accurately changed the OPD in the fiber, using both a change in refractive index and fiber path length to create an observable phase shift in a fiber based Mach Zehnder interferometer. The fiber stretcher proved to change the phase of one arm of the interferometer at least  $4\pi$  radians over an operating range of 10 kHz modulation frequency. This fiber stretcher can be controlled using a servo board, and can be incorporated into a corrective loop system to correct for phase errors in propagating light.

The injection locked amplifier used in this research proved that it can amplify injected light that matched its design wavelength, within a temperature tuned bandwidth. Operation of the amplifier is very similar to diode lasers, and is a possible source for use in a MOPA system when combined with several other amplifiers in an array. The locked

in operation of the amplifier was not affected by the fiber stretcher changing the phase of the injected beam, therefore, a combination of the two could be used to emit near infrared light with a controllable phase angle.

The fiber stretcher and injection locking amplifier used in series in this experiment has demonstrated the ability to rapidly and reliably change the phase of an amplified output beam. The combination of a large number of phase controlled beams could be constructed as a phased array of semiconductor amplifiers in order to deliver very intense light to a detector target very far away. Phase errors in propagation could be corrected at the array with the fiber stretchers using a correction and feedback loop.

## **APPENDIX A**

### **NASA Presentation**

K. Herren and K Bowman on the ring geometry for a phased array of sources.

#### **“High Power Array of Phase Locked Laser Diodes”**

**George C. Marshall Space Flight Center**

E.E. Montgomery     (Principle Investigator)

K.A. Herren

C.W. Wilkerson

E. Vaughn

K. Bowman



Electric field potential (E) of beam resulting from transmitter aperture

$$E = \frac{\epsilon_A e^{i(\omega t - kR)}}{R} \iint_{\text{Aperture}} e^{\frac{ik(Y(Y-Y_0) + Z(Z-Z_0))}{R}} ds$$

Electric field potential (E) of beam resulting from one transmitter at  $(y_0, z_0)$

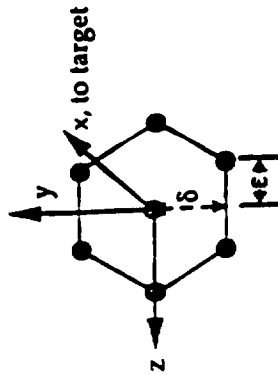
$$E_{y_0, z_0} = \frac{\epsilon_A e^{i(\omega t - kR)}}{R} e^{-\frac{ik(YY_0 + ZZ_0)}{R}} \iint_{\text{Aperture}} e^{\frac{ik(YY + ZZ)}{R}} ds$$

Combined Electric field potential (E) of beam resulting from all transmitters

$$E = \sum_{i,k} E_{y_i, z_i} e^{ik}$$

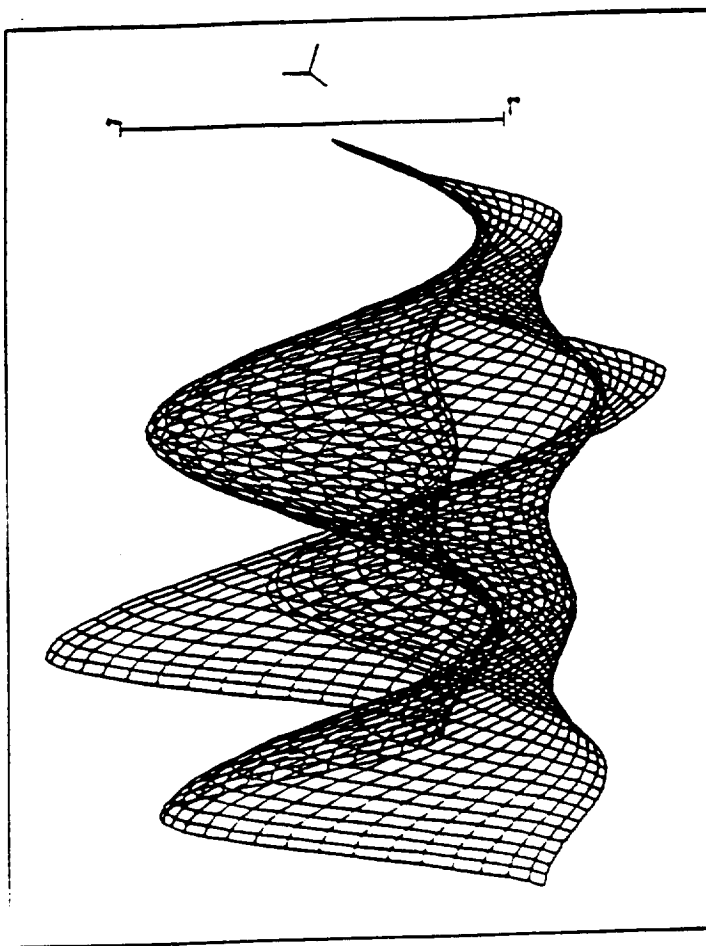
For seven transmitters in hexagonal array

$$E_{y_0, z_0} = 1 + e^{-j\pi(2Z\epsilon)} + e^{-j\pi(Y\delta + Z\epsilon)} + e^{-j\pi(-Y\delta + Z\epsilon)} + e^{-j\pi(-2Z\epsilon)} + e^{-j\pi(-Y\delta - Z\epsilon)} + e^{-j\pi(Y\delta - Z\epsilon)}$$



# Theoretical Far Field Power Distribution from One Ring of Laser Diodes

George C. Marshall  
Space Flight Center



$\lambda = 834 \text{ nm}$   
 $R = 37 \times 10^6 \text{ m}$   
 (Geostationary Orbit)  
 $\# \text{SLDs} = 7$   
 $\text{SLD power} = 1$   
 Plot Scale = 50 m X 50 m

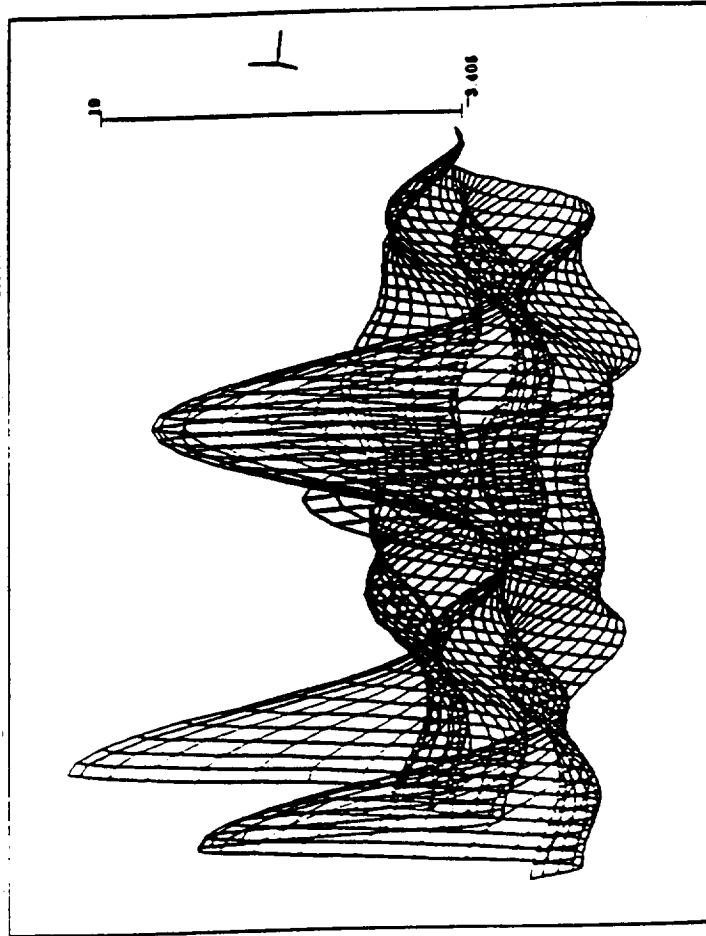
SI-MC-0094-0015



George C. Marshall  
Space Flight Center

## Theoretical Far Field Power Distribution from Two Rings of Laser Diodes

$\lambda = 834 \text{ nm}$   
 $R = 37 \times 10^6 \text{ m}$   
(Geostationary Orbit)  
#SLDs = 19  
SLD power = 1  
Plot Scale = 50 m X 50 m



E

## REFERENCES

- Andrews, J.R., Traveling-wave amplifier made from a laser diode array. *Applied Physics Letters*, **48**(20) 1986, 1311-1333.
- Andrews, J.R., Interferometric power amplifiers. *Optics Letters*. Vol. 14 No. 1, 1989, 33-35.
- Backus, C.E. "Laser Activation of Solar Cells," *Proceedings of the 9th IEEE Photovoltaic Specialists Conference*, Silver Spring, MD., May 1972.
- Born M., and Wolf, E., *Principles of Optics*, 5th edition, Pergamon Press, Elmsford, NY, 1975.
- Botez, D. and Ackley, D.E., Phase-Locked Arrays of Semiconductor Lasers. *IEEE Circuits and Devices Magazine*, January, 1986. 8-17.
- Burke, P.D., Gregory, D.A., Herren, K.A., Montgomery, E.E., "Phase correction in a semiconductor amplifier array using fiber optics," *80th Anniversary OSA Annual Meeting*, Poster session display, Rochester, NY, October 1996.
- Burke, P.D., "Phase correction using Fiber Optics," unpublished paper submitted on request to Optics and Photonics News, December 1996.
- Canadian Instrumentation and Research, *Product Data Model 915 Piezo Assembly*, Burlington, Ontario, Canada, 1995.
- Fiber Optic Trends, "Polarization preserving core structures." *Photonics Spectra Magazine*, Laurin Publishing, 1988.
- Kwon, J.H., Kim, D.H., Schuster, G. and Lee J.H., "Phase stability of injection-locked beam of semiconductor lasers." *NASA Technical Translation 10001*, February 1992.
- Kwon, J.H., Lee, J.H., and Williams, M.D., Far-field pattern of a coherently combined beam from large scale laser diode arrays. *Journal of Applied Physics*, **69**(3), 1991. 1177-1182.
- Kingsley, S.A., Method of phase-modulating signals in optical fibers: Application to optical-telemetry systems. *Electronics Letters*, Vol. 10, No. 2, 1974. 21-22.

- Kingsley, S.A., Fibredyne systems for passive or semipassive fibre-optics sensors. *Electronics Letters*, Vol. 14, No. 14, 1978. 419-422.
- Hadley, G.R., Injection Locking of Diode Lasers. *IEEE Journal of Quantum Electronics*, Vol. QE-22, No. 3, 1986. 419 - 426.
- Hecht, E., *Optics, 2nd Edition*, Addison-Wesley Publishing Company Inc., Reading, PA, 1987.
- Krohn, D.A., *Fiber Optic Sensors: Fundamentals and Applications*, Instrument Society of America, Research Triangle Park, NC, 1992.
- Kobayashi, S. and Kimura, T., Injection locking in AlGaAs semiconductor laser. *IEEE Journal of Quantum Electronics*, Vol. QE-17, No. 5, 1981. 681-689.
- Lagakos, N., Trott, W.J., Hickman, T.R., Cole, J.H. and Bucaro, J.A., Microbend fiber-optic sensor as extended hydrophone. *IEEE Journal of Quantum Electronics*, Vol. QE-18, No. 10, 1982. 1633-1638.
- Landis, G.A., Stavnes, M., Oleson, S., and Bozek, J., "Space transfer with ground-based laser/electric propulsion," *NASA Technical Memorandum 106060, 28th Joint Propulsion Conference and Exhibit*, Nashville, TN, July, 1992.
- Landis, G.A. and Westerlund, L.H., "Laser beamed power demonstration applications," *NASA Contractor Report 190793, 43rd Congress of the International Astronautical Federation*, Washington, D.C., September, 1992.
- Marathay, A.S., *Elements of Optical Coherence Theory*, John Wiley & Sons Inc., New York, NY, 1982.
- Martini, G., Analysis of a single-mode optical fibre piezoceramic phase modulator. *Optical and Quantum Electric Electronics*, 19, 1987. 179-190.
- Montgomery, E.E. and Herren, K.A., "Geostationary Power Fountain," NASA Marshall Space Flight Center distribution, December 9, 1992.
- Montgomery, E.E. (ed.), "National Advanced Optics Mission Initiative (NAOMI): Terms of Reference," NASA Marshall Space Flight Center distribution, March 10, 1995.
- Montgomery, E.E., Personal communication, 1996.
- Nussbaum, A. and Phillips, R.A., *Optics for Scientists and Engineers*, Prentice-Hall Inc., Englewood Cliffs, NJ, 1976.



Schuster, G.L. and Andrews, J.R., Coherent summation of saturated AlGaAs amplifiers. *Optics Letters*, Vol. 18, No. 8, 1993. 619-621.

Udd, E., *Fiber Optic Sensors: An introduction for engineers and scientists*, John Wiley & Sons Inc., New York, NY, 1991.

Walker, G.H. and Heinbockel, J.H., Mathematical optimization of photovoltaic converters for diode lasers. *Proceedings of the 24th Intersociety Energy Conversion Engineering Conference*, Washington, D.C., August 1989.

Wang, W., Nakagawa, K., Sayama, S., Ohtsu, M., Coherent addition of injection-locked high-power AlGaAs diode lasers. *Optics Letters*, Vol. 17, No. 22, 1992. 1593-1595.

Williams, M.D., Laser power beams obtained by the dynamic selection of emitting elements in an array. *Applied Optics*, Vol.31, No. 15, 1992. 2738-2742.

Yoshino, T., Kurosawa, K., Itoh, K. and Ose, T., Fiber-optic Fabry-Perot interferometer and its sensor applications. *IEEE Journal of Quantum Electronics*, Vol. QE-18, No. 10, 1982. 1624-1633.

## BIBLIOGRAPHY

Goodman, J.W., *Introduction to Fourier Optics*, McGraw-Hill Incorporated, New York, New York, 1968.

Pedrotti, F.L. and Pedrotti, L.S., *Introduction to Optics*, Prentice-Hall, Inc., Englewood Cliffs, New Jersey, 1987.

# Report Document Page

<b>1. Report No.</b>		<b>2. Government Accession No.</b>		<b>3. Recipients Catalog No.</b>	
<b>4. Title and Subtitle</b> Investigation of Fiber Optics Based Phased Locked Diode Lasers				<b>5. Report Due</b> March 14, 1996	
				<b>6. Performing Organization Code</b> UAH	
<b>7. Author(s)</b> Paul D. Burke Don A. Gregory, Pricipal Investigator				<b>8. Performing Organization Report No.</b>	
				<b>10. Work Unit No.</b>	
<b>9. Performing Organization Name and Address</b> University of Alabama in Huntsville Department of Physics Huntsville, AL 35899				<b>11. Contract or Grant No.</b> NAS8-38609 D.O. 138	
				<b>13. Type of report and Period covered</b> Final	
<b>12. Sponsoring Agency Name and Address</b> NASA Marshall Space Flight Center Huntsville, Al				<b>14. Sponsoring Agency Code</b>	
				<b>15. Supplementary Notes</b>	
<b>16. Abstract</b> <p>Optical power beaming requires a high intensity source and a system to address beam phase and location. A synthetic aperture array of phased locked sources can provide the necessary power levels as well as a means to correct for phase errors. A fiber optic phase modulator with a master oscillator and power amplifier (MOPA) using an injection-locking semiconductor optical amplifier has proven to be effective in correcting phase errors as large a <math>4\pi</math> in an interferometer system. Phase corrections with the piezo electric fiber stretcher were made from 0 - 10 kHz, with most application oriented corrections requiring only 1 kHz. The amplifier did not lose lose locked power output while the phase was changed, however its performance was below expectation. Results of this investigation indicate fiber stretchers and amplifiers can be incorporated into a MOPA system to achieve successful earth based power beaming.</p>					
<b>17. Key Words (Suggested by Author (s))</b> Fiber Optics Phase Correction Power Beaming				<b>18. Distribution Statement</b>	
<b>19. Security Class. (of this report)</b> Unclassified		<b>20. Security Class. (of this page)</b> Unclassified		<b>21. No. of pages</b>	
				<b>22. Price</b>	